

Beyond One-Size-Fits-All: Tailored Benchmarks for Efficient Evaluation

Anonymous ACL submission

Abstract

Evaluating models on large benchmarks is very resource-intensive, especially during the period of rapid model evolution. Existing efficient evaluation methods estimate the performance of target models by testing them only on a small and static coreset of benchmark, which is derived from the publicly available evaluation results of source models. These methods rely on the assumption that target models have high prediction consistency with source models. However, we demonstrate that it doesn't generalize well in practice. To alleviate the inconsistency issue, we present TAILOREDBENCH, a method that conducts customized evaluation tailored to each target model. Specifically, a Global-coreset is first constructed as a probe to identify the most consistent source models for each target model with an adaptive source model selection strategy. Afterwards, a scalable K-Medoids clustering algorithm is proposed to extend the Global-coreset to a tailored Native-coreset for each target model. According to the predictions on Native-coresets, we obtain the performance of target models on the whole benchmark with a calibrated estimation strategy. Comprehensive experiments on 5 benchmarks across over 300 models demonstrate that compared to best performing baselines, TAILOREDBENCH achieves an average reduction of 31.4% in MAE of accuracy estimates under the same inference budgets, showcasing strong effectiveness and generalizability.

1 Introduction

Scaling up models in multiple dimensions has led to remarkable advancements in their capabilities (Touvron et al., 2023; Ouyang et al., 2022), which also presents significant challenges for efficiently assessing them. For instance, Liang et al. (2022) reports that evaluating a model with approximately 10 billion parameters on the HELM leaderboard costs over \$1,700 via APIs or more than 1,200

GPU hours. Moreover, these costs scale by a factor of X when exploring and comparing X different training or inference configurations during the development or deployment phase.

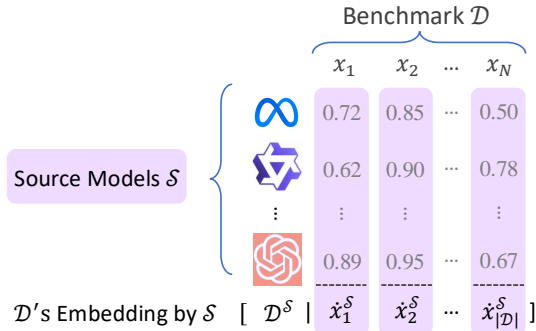
To achieve efficient evaluation, some studies (Vivek et al., 2024; Polo et al., 2024) have explored the following paradigm: *step 1.* constructing example embeddings according to the predictions from a set of *source models* (which are freely available for popular leaderboards^{1,2,3}); *step 2.* clustering the benchmark and selecting the cluster centroids to form a coreset (typically less than 100 examples); *step 3.* approximating the performance of *target models* under evaluation based on their predictions on the coreset. (See detailed related works in Appendix A.) Underlying this approach is the assumption that performance patterns generalize: if source models respond similarly to two examples a and b , then a target model's performance on a can be used to estimate its performance on b .

Nevertheless, we find that such generalizability between source and target models does not necessarily hold. Following ANCHORPOINT (Vivek et al., 2024), we construct an embedding based on the correctness (e.g., the probability of the correct option) of all source models for each example and visualize them using t-SNE algorithm (Van der Maaten and Hinton, 2008). In these embeddings (Figure 1a), nearby examples elicit similar predictions from the source models, allowing cluster centroids (marked by stars) to serve as representative points. Yet, when we adopt embeddings derived from the correctness of target models instead (Figure 1b), the average distance between the example and its centroid increases from 10.09 to 12.48, indicating that the previously chosen centroids fail to represent their respective clusters effectively. This reveals a discrepancy in prediction behaviors be-

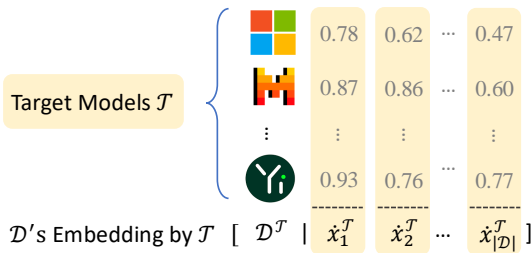
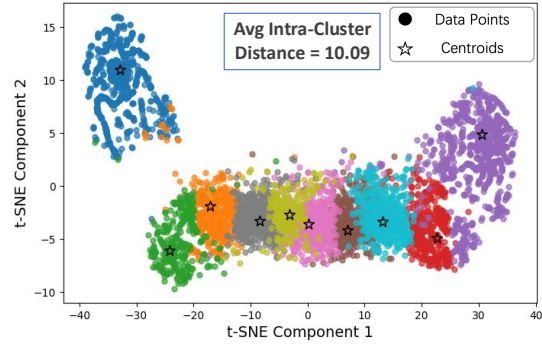
¹<https://huggingface.co/open-llm-leaderboard>

²<https://rank.opencompass.org.cn>

³<https://crfm.stanford.edu/helm>



(a) Hellaswag benchmark represented by source-model embeddings $\mathcal{D}^{\mathcal{S}}$.



(b) Hellaswag benchmark represented by target-model embeddings $\mathcal{D}^{\mathcal{T}}$.

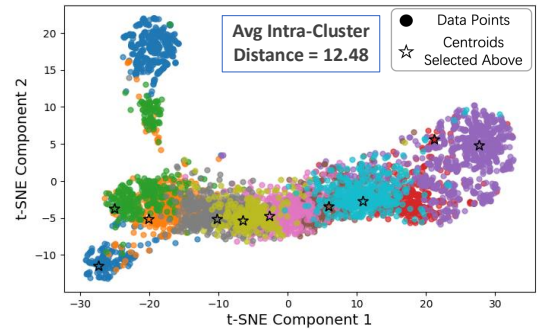


Figure 1: The t-SNE visualization of the Hellaswag benchmark using embeddings derived from source (above) and target (below) models’ predictions. The increased average distance between examples and their cluster centroids in the target-based embedding indicates that the coreset (centroids) obtained from source-based embeddings no longer effectively represents the entire benchmark for target models.

081 between source and target models, which we term
 082 *prediction consistency*—the extent to which their
 083 predictions align on the same examples. When pre-
 084 diction consistency is low, source-model-derived
 085 coresets fail to generalize, resulting in inaccurate
 086 performance estimates for target models.

087 To address the aforementioned issue, we pro-
 088 pose the TAILOREDBENCH method, which adap-
 089 tively constructs model-specific evaluation coreset
 090 in a global to native manner for accurate and effi-
 091 cient evaluation. Specifically, we first construct a
 092 static G-set (Global-coreset) based on the predic-
 093 tion results of all the source models. By applying
 094 an adaptive source model selection strategy, the
 095 predictions of target models on the G-set are used
 096 as a probe to select a native source model set for
 097 each target model that has stronger prediction con-
 098 sistency with them. Based on this posterior, we
 099 design a scalable K-Medoids clustering technique
 100 to expand the G-set into an N-set (Native-coreset)
 101 for each target model, according to the benchmark
 102 embeddings under the metric of corresponding na-
 103 tive source models. Finally, we approximate the
 104 overall performance of target models by employ-
 105 ing a calibrated estimation strategy based on their

predictions on the N-set. 106

107 We conduct extensive experiments on five bench-
 108 marks across more than 300 models, involving
 109 tasks in the fields of natural language and multi-
 110 modality. Compared to non-customized efficient
 111 evaluation baselines, TAILOREDBENCH can more
 112 accurately estimate the performance of models (at-
 113 taining an average of 31.4% MAE degradation
 114 improvement on accuracy) under the same small-
 115 size inference budgets (generally 20~40 examples).
 116 Our contributions are summarized as follows:

- 117 • We analyze that the existing efficient evalua-
 118 tion methods overestimate the prediction con-
 119 sistency across models, thus the source-model-
 120 based static coreset may fail to assess the tar-
 121 get models accurately. 121
- 122 • We propose the TAILOREDBENCH method to
 123 conduct tailored evaluation on adaptively con-
 124 structed N-set for each target model to attain
 125 more accurate evaluation results. 125
- 126 • We conduct comprehensive experiments and
 127 analyses on multiple settings to validate the
 128 excellent effectiveness and strong generaliz-
 129 ability of TAILOREDBENCH. 129

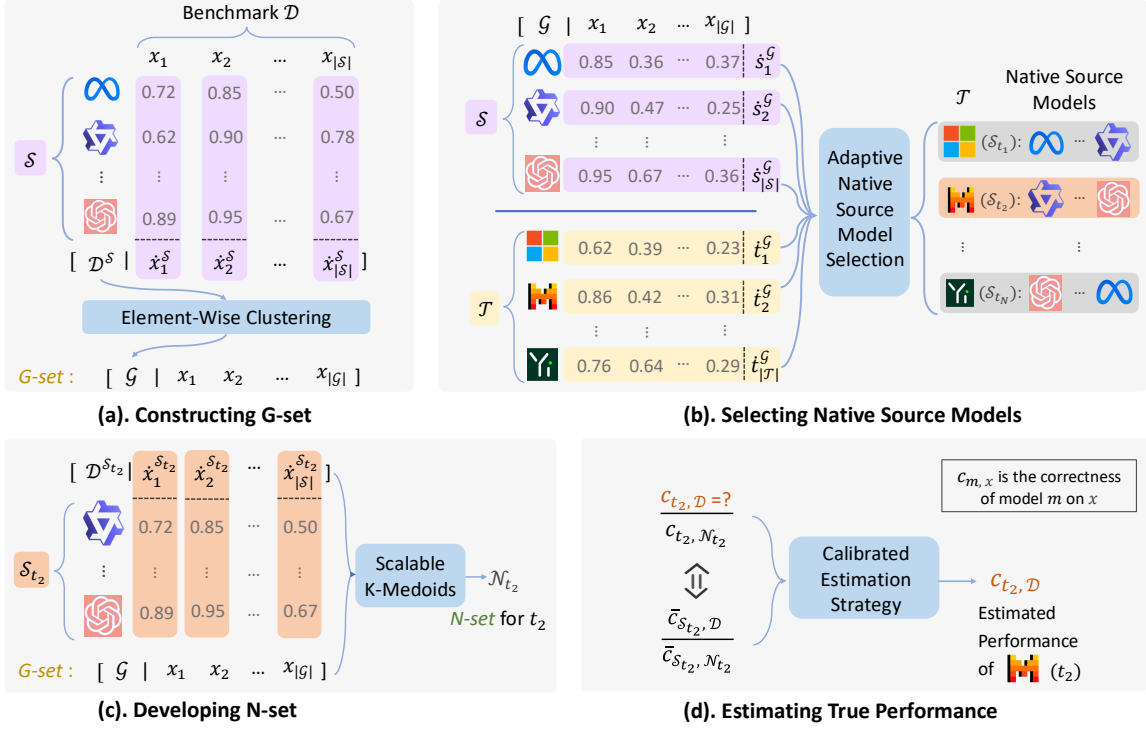


Figure 2: Overview of TAILOREDBENCH.

2 TailoredBench Approach

The TAILOREDBENCH approach centers on dynamically selecting prediction-consistent source models and crafting an N-set that faithfully represents the entire benchmark for each target model. Its formulation proceeds through four tightly integrated steps: constructing a globally representative G-set (§2.2), identifying native source models (§2.3) and developing N-set for each target model (§2.4), and finally estimating the target models’ overall performance (§2.5).

2.1 Task Set-Up

Let $\mathcal{D} = \{(x_k, y_k)\}_{k=1}^{|\mathcal{D}|}$ denotes a benchmark, where x_k is the input and y_k is the corresponding ground truth output. We define the set of target models under evaluation as $\mathcal{T} = \{t_m\}_{m=1}^{|\mathcal{T}|}$. Additionally, we denote the source model set as $\mathcal{S} = \{s_n\}_{n=1}^{|\mathcal{S}|}$, for which we have access to their predictions across all examples in \mathcal{D} . Following previous works, we ensure that $\mathcal{T} \cap \mathcal{S} = \emptyset$. Our objective is to accurately estimate the performance P_{t_m} of each target model $t_m \in \mathcal{T}$ and determine the ranking relationships within \mathcal{T} , while minimizing the model inference cost.

2.2 Constructing G-set

We first construct the G-set \mathcal{G} , which is designed as a probe for each target model to identify a set of source models with the highest prediction consistency. Consequently, it is intended to be a small yet relatively representative subset of the benchmark, ensuring its generalizability across target models.

Following prior works (Vivek et al., 2024), we employ clustering based on the correctness of source models to construct the G-set. Here, correctness can be either the predictive probability of the correct option (continuous value $[0, 1]$) or whether the model answers the example correctly (discrete binary value $\{0, 1\}$).

Leveraging the correctness scores c_{s_n, x_k} of each source model s_n on the example x_k , we embed the benchmark \mathcal{D} into $\mathcal{D}^{\mathcal{S}} = \{\dot{x}_k^{\mathcal{S}}\}_{k=1}^{|\mathcal{D}|}$ as follows:

$$\dot{x}_k^{\mathcal{S}} = \begin{pmatrix} c_{s_1, x_k} \\ c_{s_2, x_k} \\ \vdots \\ c_{s_{|\mathcal{S}|}, x_k} \end{pmatrix} \quad (1)$$

where \dot{x}_k represents the embedding of x_k , with the superscript \mathcal{S} indicating that it is derived from source models’ correctness.

Based on $\mathcal{D}^{\mathcal{S}}$, we apply K-Medoids clustering (Kaufman and Rousseeuw, 2009) to select the G-

set with the objective function below:

$$\min_{\{\mathcal{G}, \mathcal{C}_g\}} \sum_{x_g \in \mathcal{G}} \sum_{x_k \in \mathcal{C}_g \setminus \{x_g\}} \text{Dis}(x_g^{\mathcal{S}}, x_k^{\mathcal{S}}) \quad (2)$$

where x_g is an example in the G-set $\mathcal{G} = \{x_g\}_{g=1}^{|\mathcal{G}|}$, and \mathcal{C}_g is the cluster for which x_g is the centroid. Dis denotes the distance metric in clustering.

To maximize the generalization capability of our method, the choice of distance metric is critical. Previous approaches (Vivek et al., 2024; Miller et al., 2021; Baek et al., 2022; Mehra et al., 2024) using correlation distance (Rodgers and Nicewander, 1988) to measure example consistency often assume linear relationships in scoring patterns among models or examples. However, this assumption may not hold for discrete numerical embeddings, leading to significant performance degradation. In contrast, element-wise distance (e.g., Manhattan distance) can effectively capture individual discrepancies in correctness vectors, thereby accommodating various correctness formats. We compare three types of distance in Table 2, demonstrating the superiority of element-wise metrics. By default, we adopt Manhattan distance as Dis for our TAILOREDBENCH method.

2.3 Adaptive Native Source Model Selection

After constructing G-set \mathcal{G} , we attain the prediction results of target models \mathcal{T} on it, which we use as a probe to construct a Native Source Model Set \mathcal{S}_{t_m} that exhibits the highest prediction consistency for each $t_m \in \mathcal{T}$.

Specifically, we first embed all the source models $s_n \in \mathcal{S}$ and target models $t_m \in \mathcal{T}$ based on their prediction correctness on \mathcal{G} as follows:

$$\dot{s}_n^{\mathcal{G}} = \begin{pmatrix} c_{s_n, x_1} \\ c_{s_n, x_2} \\ \vdots \\ c_{s_n, x_{|\mathcal{G}|}} \end{pmatrix}, \quad \dot{t}_m^{\mathcal{G}} = \begin{pmatrix} c_{t_m, x_1} \\ c_{t_m, x_2} \\ \vdots \\ c_{t_m, x_{|\mathcal{G}|}} \end{pmatrix} \quad (3)$$

Here, the superscript \mathcal{G} indicates that each dimension of the vector is derived from the model’s prediction correctness on the G-set. Leveraging these vectors, we compute the average prediction consistency \bar{d} among all the models (both source and target) on the G-set as follows:

$$\bar{d} = \frac{2}{(|\mathcal{S}| + |\mathcal{T}|)(|\mathcal{S}| + |\mathcal{T}| - 1)} \sum_{i < j} d_{ij}, \quad (4)$$

where $d_{ij} = \text{Dis}(\dot{\phi}_i^{\mathcal{G}}, \dot{\phi}_j^{\mathcal{G}})$

In this context, $i, j \in [1, |\mathcal{S}| + |\mathcal{T}|]$ and ϕ represents any model from $\mathcal{S} \cup \mathcal{T}$. By computing \bar{d} across all models, we establish a robust threshold that reflects the model set’s similarity landscape, enabling consistent and effective selection of native source models for each target model.

On this basis, we determine \bar{n} , the size of the native source model set for target models, by calculating the average number of source models whose prediction consistency with each target model exceeds the threshold \bar{d} as follows:

$$\bar{n} = \left\lfloor \frac{1}{|\mathcal{T}|} \sum_{m=1}^{|\mathcal{T}|} |\mathcal{S}_{t_m}| \right\rfloor, \quad (5)$$

$$\text{where } \mathcal{S}_{t_m} = \left\{ s_n \in \mathcal{S} \mid \text{Dis}(\dot{s}_n^{\mathcal{G}}, \dot{t}_m^{\mathcal{G}}) < \bar{d} \right\}$$

For a target model t_m , the top \bar{n} source models exhibiting the highest prediction consistency are selected to form its dynamic source model set \mathcal{S}_{t_m} . By standardizing the number of native source models across all target models, we ensure that each target model’s feature representation maintains consistent dimensionality and informational richness during subsequent clustering.

2.4 Developing N-set

Leveraging the selected native source models \mathcal{S}_{t_m} , we construct the most representative N-set \mathcal{N}_{t_m} for each target model t_m . To maximize the utilization of the observed prediction results of target models on \mathcal{G} , we propose a SCALABLE K-MEDOIDS CLUSTERING algorithm to extend \mathcal{G} into the N-set.

Initially, each example $x_k \in \mathcal{D}$ is represented by a feature vector $x_k^{\mathcal{S}_{t_m}}$, which is based on the correctness of its native source models \mathcal{S}_{t_m} . Then, our SCALABLE K-MEDOIDS CLUSTERING algorithm operates as follows:

Anchored Medoid Initialization: Fix the examples in G-set as initial medoids. If the desired N-set size is $|\mathcal{N}_{t_m}|$ and the G-set contains $|\mathcal{G}|$ examples, we randomly select $|\mathcal{N}_{t_m}| - |\mathcal{G}|$ additional examples from $\mathcal{D} \setminus \mathcal{G}$ to form the initial medoid set.

Cluster Assignment: Assign each example $x_k \in \mathcal{D}$ to the nearest medoid x_μ to form the cluster \mathcal{C}_μ :

$$x_k \in \mathcal{C}_\mu, \quad \text{where } \mu = \arg \min_{\mu} \text{Dis}(x_\mu^{\mathcal{S}_{t_m}}, x_k^{\mathcal{S}_{t_m}}) \quad (6)$$

Dynamic Medoid Refinement: For each cluster \mathcal{C}_μ with a non-G-set medoid, update the medoid x_μ by selecting the example within \mathcal{C}_μ that minimizes the total distance to all other examples in \mathcal{C}_μ :

$$x_\mu = \arg \min_{x_i \in \mathcal{C}_\mu} \sum_{x_j \in \mathcal{C}_\mu \setminus \{x_i\}} \text{Dis}(x_i^{S_{t_m}}, x_j^{S_{t_m}}) \quad (7)$$

Medoids corresponding to G-set remain fixed during this process.

Convergence Verification: Repeat the Cluster Assignment and Dynamic Medoid Refinement steps until convergence is achieved, i.e., when medoids no longer change or a maximum number of iterations is reached.

By incorporating the G-set examples as fixed medoids, the clustering process ensures that these pivotal examples guide the formation of clusters and the selection of additional N-set examples.

2.5 Calibrated Performance Estimation

After establishing the N-set \mathcal{N}_{t_m} for a target model t_m , for previous methods (Vivek et al., 2024; Polo et al., 2024), they may estimate the model’s overall performance by first evaluating it on these centroid examples and then weighting the results according to each centroid’s coverage of the benchmark. However, simply relying on medoids overlooks subtle variations in how individual examples within each cluster are predicted, potentially leading to less accurate global estimates.

To address this, we leverage the prediction consistency between the target model t_m and its native source models \mathcal{S}_{t_m} to obtain the calibrated correctness estimates for the target model. For a given cluster with medoid x , consider any non-medoid example x' in the same cluster. We compute a scaling factor based on the native source models’ average correctness, which reflects how the prediction patterns at x' relate to those at x :

$$\text{Scale}(x') = \frac{\bar{c}_{\mathcal{S}_{t_m}, x'} + 0.5}{\bar{c}_{\mathcal{S}_{t_m}, x} + 0.5} \quad (8)$$

Here, $\bar{c}_{\mathcal{S}_{t_m}, x}$ and $\bar{c}_{\mathcal{S}_{t_m}, x'}$ denote the average correctness of \mathcal{S}_{t_m} on the medoid x and the non-medoid x' , respectively. The addition of 0.5 ensures numerical stability by preventing the denominator from becoming zero. Given that t_m and \mathcal{S}_{t_m} exhibit similar prediction consistencies, we assume this scaling factor can be applied to estimate the target model’s correctness on x' :

$$c_{t_m, x'} = (c_{t_m, x} + 0.5) \cdot \text{Scale}(x') - 0.5 \quad (9)$$

By integrating these inferred correctness values across all examples in the benchmark \mathcal{D} , we obtain a more faithful global performance estimation without re-evaluating the entire dataset:

$$P_{t_m} = \frac{1}{|\mathcal{D}|} \sum_{x' \in \mathcal{D}} c_{t_m, x'} \quad (10)$$

3 Experiments

3.1 Experimental Setup

Benchmarks and Models We validate TAILOREDBENCH on five diverse benchmarks spanning natural language and multimodal tasks. ARC Challenge (Clark et al., 2018) consists of 1,172 scientific reasoning questions, with predictions from 153 models. Hellaswag (Zellers et al., 2019) provides 6,000 commonsense inference examples (a subset of its validation set) and outputs from 139 models. GSM8K (Cobbe et al., 2021) includes 1,319 math reasoning problems tested on 150 models. Winogrande (Sakaguchi et al., 2021) has 1,267 pronoun resolution examples with 150 models evaluated. POPE (Li et al., 2023) features 5,127 instances for assessing multimodal hallucination, accompanied by results from 99 models. A complete list of models used for each benchmark is provided in Appendix C. We randomly split models into source and target sets for each benchmark, ensuring that their intersection is empty.

For ARC Challenge and Hellaswag, model correctness is represented by continuous probabilities, while GSM8K, Winogrande, and POPE use binary correctness $\{0, 1\}$. Predictions for ARC Challenge, Hellaswag, GSM8K, and Winogrande come from the Open LLM Leaderboard (Beeching et al., 2023), and those for POPE are from the OpenCompass Leaderboard (Contributors, 2023).

Baseline and Evaluation Metrics We compare TAILOREDBENCH against three baselines: a *Random Sampling* strategy that randomly selects a subset of examples from the benchmark to estimate model performance, serving as a basic reference point; the *Anchor Points* method (Vivek et al., 2024), which uses K-Medoids clustering on source-model predictions to identify a fixed representative coreset; and *gp-IRT* (Polo et al., 2024), which employs an Item Response Theory model trained on the predictions of the source models to estimate target models’ performance on the full benchmark. In all cases, we use the same source models and target models to ensure a fair comparison.

Benchmarks	Inference counts	20		25		30		35		40	
		$\tau \uparrow$	MAE \downarrow	$\tau \uparrow$	MAE \downarrow	$\tau \uparrow$	MAE \downarrow	$\tau \uparrow$	MAE \downarrow	$\tau \uparrow$	MAE \downarrow
ARC Challenge	BEST BASELINE	0.662	0.046	0.663	0.046	0.676	0.036	0.713	0.036	0.714	0.029
	TAILOREDBENCH	0.711	0.031	0.737	0.029	0.756	0.028	0.766	0.027	0.773	0.027
Hellaswag	BEST BASELINE	0.860	0.060	0.880	0.053	0.877	0.043	0.897	0.038	0.898	0.032
	TAILOREDBENCH	0.900	0.020	0.909	0.018	0.913	0.018	0.914	0.017	0.918	0.017
GSM8K	BEST BASELINE	0.811	0.055	0.828	0.047	0.839	0.041	0.847	0.038	0.858	0.034
	TAILOREDBENCH	0.852	0.035	0.858	0.034	0.863	0.033	0.869	0.031	0.878	0.029
Winogrande	BEST BASELINE	0.472	0.041	0.487	0.038	0.514	0.038	0.521	0.036	0.518	0.034
	TAILOREDBENCH	0.565	0.028	0.568	0.026	0.604	0.024	0.608	0.023	0.618	0.022
POPE	BEST BASELINE	0.488	0.038	0.510	0.037	0.518	0.034	0.547	0.033	0.556	0.031
	TAILOREDBENCH	0.521	0.036	0.547	0.035	0.562	0.031	0.563	0.031	0.574	0.032

Table 1: Results on all benchmarks. For each setting, we take the best result from multiple baselines to compare with TAILOREDBENCH. The detailed performance of each baseline under each setting is presented in Table 6. Values in bold represent the best results.

We employ two metrics to assess these methods. *Kendall’s τ Correlation Coefficient* evaluates the ordinal agreement between estimated and true model rankings, indicating how well the relative performance order is preserved. *Mean Absolute Error (MAE)* measures the average absolute deviation between estimated and true performance scores, thereby capturing the precision of performance estimation for individual target models.

3.2 Main Results

TailoredBench: Effective Ranking and Estimation of Model Performances Tables 1 present a comprehensive comparison between our TAILOREDBENCH method and the best baseline approaches for each metric across all benchmarks. Full results are available in Appendix B.1. In our experiments, we allocated 10 examples to the G-set and averaged the outcomes over 100 randomized trials to ensure statistical reliability. The inference count—defined as the number of examples in the N-set for our method—varied from 20 to 40.

As demonstrated in the tables, our method consistently outperforms baseline approaches in both Kendall’s τ and MAE metrics across all inference counts and benchmarks featuring different correctness types. When the inference count increases, the performance of our method continues to improve, evidenced by a steady increase in Kendall’s τ and a continuous decrease in MAE. Notably, compared to best performing baselines, our approach achieves nearly a 31.4% reduction in MAE. These results indicate that our method effectively estimates the relative performance among target models and provides more accurate estimations of their performance on the entire benchmark. Fur-

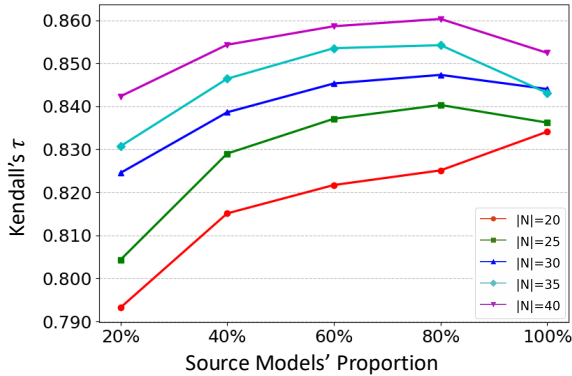
thermore, compared to the static AnchorPoints method, our approach significantly improves both Kendall’s τ and MAE metrics, highlighting its effectiveness in adaptively selecting a more representative N-set for each target model and thereby improving estimation accuracy. We also calculate the accuracy of our method in ranking the performance between every pair of target models. The results show that the accuracy reached 96.0% on the Hellaswag benchmark and 93.6% on the GSM8K benchmark. In terms of robustness, Appendix B.6 demonstrates that our method exhibits significantly lower variance compared to the baselines.

Moreover, across all benchmarks and inference counts, we conduct a one-sided Z-test over 100 repeated experiments. Whenever our method outperformed the baselines, the p-values remained below 0.05, confirming a statistical advantage.

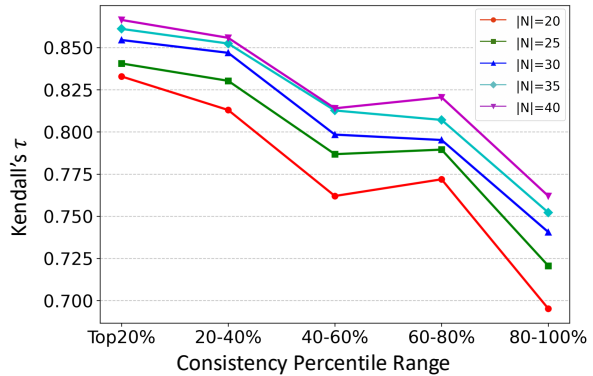
3.3 Ablation Studies

Element-Wise Distance Effectively Facilitates Handling Various Data Forms Our method uses element-wise Distance (specifically Manhattan distance) to effectively handle both continuous and discrete values. As shown in Table 2, with 30 inference counts, element-wise Distances outperform the correlation distance used by AnchorPoints. This confirms its effectiveness in improving our method’s performance. Detailed per-dataset results are provided in Appendix B.5.

Calibrated Estimation Strategy Improves Performance Estimation We compare TAILOREDBENCH with and without calibration. As shown in Table 3, with 30 inference counts, the calibrated variant achieves higher Kendall’s τ and lower MAE, confirming that calibration enhances



(a) The impact of the quantity of Native Source Models (with prediction consistency kept the same).



(b) The impact of prediction consistency between the Native Source Model and Target Model (with quantity kept the same).

Figure 3: Investigating the impact of native source model quantity and prediction consistency with target model on GSM8K using the controlled variable method.

Distance	$\tau \uparrow$	MAE \downarrow
CORRELATION	0.720	0.032
COSINE	<u>0.736</u>	<u>0.028</u>
MANHATTAN	0.740	0.027

Table 2: Average performance with different types of distance across benchmarks.

the accuracy of performance estimation. Detailed per-dataset results are provided in Appendix B.2.

3.4 Analyses

Impact of Native Source Model Selection on Method Performance Here, we isolate the effects of both the number of native source models and their prediction consistency with the target model by independently varying these factors, without applying our adaptive native source model selection mechanism.

When native source models share a fixed level of prediction consistency with the target model, increasing their number enhances performance. To investigate this, we randomly select models designated as native source models, from 20% to 100%. As shown in Figure 3a, performance improves as more native source models are included, since a larger set of models offers a greater chance of obtaining a more robust embedding. See Appendix B.7 for results on more benchmarks.

When the number of native source models is fixed, higher prediction consistency with the target model enhances performance. To examine this, we select a fixed number of native source models at various consistency levels relative to the target model (top 20%, 20~40%, up to 80~100%). As shown in Figure 3b (with the horizontal axis repre-

Method Variants	$\tau \uparrow$	MAE \downarrow
NON-CALIBRATED	0.724	0.030
CALIBRATED	0.740	0.027

Table 3: Average performance with and without calibration across benchmarks.

sending the Consistency Percentile Range for these intervals), Kendall's τ decreases sharply as the consistency percentile range expands. See Appendix B.8 for additional benchmark results.

TailoredBench Method Adaptively Selects Optimal Native Source Model Sets

Here, we analyze the ability of our method to select the optimal native source model sets. Figure 4 shows the performance of our method on the GSM8K benchmark, where source models with the top-k prediction consistency to the target model are selected as Native source models. The results reveal that Kendall's τ coefficient initially increases and then decreases as the number of native source models grows, while the MAE first decreases and then increases. This trend aligns with our observations in Figure 3. Specifically, when only a few native source models are selected, their high consistency with the target model is offset by the noise introduced due to the small sample size, which reduces clustering performance. Increasing the number of native source models helps mitigate this issue and improves performance until an optimal point is reached. However, selecting too many native source models incorporates models with lower prediction consistency to the target model, which diminishes effectiveness. Our method addresses this by adaptively selecting the near-optimal number of native source models across all benchmarks. For

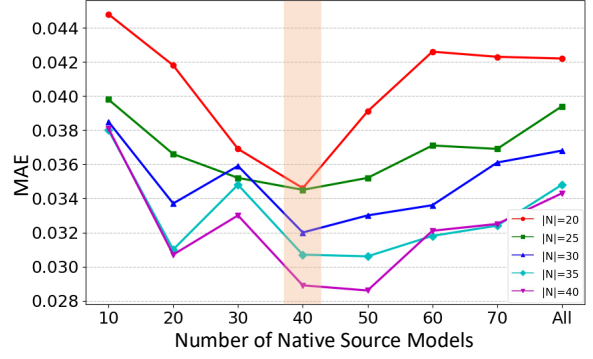
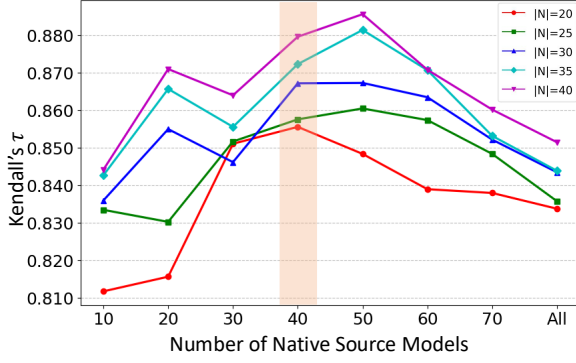


Figure 4: Performance of TAILOREDBENCH with varying numbers of Native Source Models on GSM8K benchmark. The shaded area indicates the adaptively selected number of native source models and the corresponding performance of our method.

example, as shown in Figure 4, our approach selects 40 native source models for each target model on the GSM8K benchmark, achieving near-optimal performance. Further experiments pertaining to this section are detailed in Appendix B.9.

Additionally, we observe that target models preferentially select native source models from their own family, which can better capture the nuances and prediction patterns distinctive to their respective model lineages and contribute to more accurate performance estimations. This intra-family selection bias is explored in detail in Appendix B.3.

10 Examples are Sufficient for the Probe We investigate how G-set size affects our method’s performance by fixing the N-set at 30 examples and varying the G-set from 5 to 25 examples across all benchmarks. As shown in Table 4, Kendall’s τ peaks and MAE reaches a minimum at a G-set size of 10. Smaller G-set fail to capture the prediction consistency between source and target models, limiting effective N-set selection. Conversely, a larger G-set reduces N-set representativeness by being dominated by G-set points, leading to diminished performance. Detailed per-dataset results are provided in Appendix B.4.

G-set	$\tau \uparrow$	MAE \downarrow
5	0.734	0.030
10	0.740	0.027
15	<u>0.736</u>	<u>0.028</u>
20	0.735	<u>0.028</u>
25	0.731	0.029

Table 4: Average performance with different G-set size across benchmarks.

Performance with Larger Inference Count On the Hellaswag Benchmark. We further evalu-

ate our method with larger inference counts on the Hellaswag benchmark. As shown in Table 5, as the inference counts increase from 50 to 150, TAILOREDBENCH consistently achieves improvements in model performance prediction and ranking, maintaining a clear advantage over various baseline methods. This demonstrates that TAILOREDBENCH generalizes effectively to larger inference budgets.

Inference counts	50		100		150	
	$\tau \uparrow$	MAE \downarrow	$\tau \uparrow$	MAE \downarrow	$\tau \uparrow$	MAE \downarrow
RANDOM	0.887	0.053	0.920	0.038	0.935	<u>0.030</u>
ANCHOR POINTS	<u>0.915</u>	0.046	<u>0.931</u>	0.040	<u>0.940</u>	0.040
GP-IRT	0.869	<u>0.026</u>	0.915	<u>0.015</u>	0.936	0.012
TAILOREDBENCH	0.923	0.016	0.934	0.014	0.943	0.012

Table 5: Performance of compared methods on the Hellaswag benchmark with larger inference counts.

4 Conclusions

In this paper, we propose the TAILOREDBENCH method, which mainly includes an adaptive source model set selection strategy, a scalable K-Medoids clustering algorithm and a calibrated performance estimation strategy. Abandoning the one-size-fits-all approach, we have customized the evaluation on the constructed native coreset for each target model. This approach enables a more accurate reconstruction and ranking of the model’s performance on the entire benchmark with a small-size inference budget. Comprehensive experiments show that TAILOREDBENCH can achieve more accurate model evaluation (an average of 31.4% estimation MAE loss degradation) with few inference costs.

528 Limitations

529 A primary limitation of mainstream approaches in
530 benchmark compression, including (Vivek et al.,
531 2024; Polo et al., 2024), and our method, is their
532 dependence on comprehensive evaluation results
533 from existing models across all examples within a
534 benchmark. As described above, these results are
535 typically readily accessible through public leader-
536 boards. However, obtaining initial model perfor-
537 mance results is necessary for new or certain pri-
538 vate benchmarks, which introduces additional in-
539 ference overhead. Nonetheless, we maintain that
540 this initial cost is justified, as it is offset by the
541 significant resource savings achieved through nu-
542 merous subsequent rapid evaluations facilitated by
543 our method.

544 Ethics Statement

545 All of the datasets used in this study were publicly
546 available, and no annotators were employed for our
547 data collection. We confirm that the datasets we
548 used did not contain any harmful content and was
549 consistent with their intended use (research). We
550 have cited the datasets and relevant works used in
551 this study.

552 References

553 Anas Awadalla, Mitchell Wortsman, Gabriel Ilharco,
554 Sewon Min, Ian Magnusson, Hannaneh Hajishirzi,
555 and Ludwig Schmidt. 2022. Exploring the landscape
556 of distributional robustness for question answering
557 models. arXiv preprint arXiv:2210.12517.

558 Christina Baek, Yiding Jiang, Aditi Raghunathan, and
559 J Zico Kolter. 2022. Agreement-on-the-line: Pre-
560 dicting the performance of neural networks under
561 distribution shift. Advances in Neural Information
562 Processing Systems, 35:19274–19289.

563 Edward Beeching, Clémentine Fourier, Nathan Habib,
564 Sheon Han, Nathan Lambert, Nazneen Rajani, Omar
565 Sanseviero, Lewis Tunstall, and Thomas Wolf. 2023.
566 Open llm leaderboard. [https://huggingface.co/
567 spaces/open-llm-leaderboard-old/open_llm_
568 leaderboard](https://huggingface.co/spaces/open-llm-leaderboard-old/open_llm_leaderboard).

569 Peter Clark, Isaac Cowhey, Oren Etzioni, Tushar Khot,
570 Ashish Sabharwal, Carissa Schoenick, and Oyvind
571 Taffjord. 2018. Think you have solved question
572 answering? try arc, the ai2 reasoning challenge. arXiv
573 preprint arXiv:1803.05457.

574 Karl Cobbe, Vineet Kosaraju, Mohammad Bavarian,
575 Mark Chen, Heewoo Jun, Lukasz Kaiser, Matthias
576 Plappert, Jerry Tworek, Jacob Hilton, Reiichiro
577 Nakano, et al. 2021. Training verifiers to solve math
578 word problems. arXiv preprint arXiv:2110.14168.

OpenCompass Contributors. 2023. Opencompass: 579
A universal evaluation platform for foundation 580
models. [https://github.com/open-compass/](https://github.com/open-compass/opencompass) 581
[opencompass](https://github.com/open-compass/opencompass). 582

Shengding Hu, Xin Liu, Xu Han, Xinrong Zhang, Chao- 583
qun He, Weilin Zhao, Yankai Lin, Ning Ding, Zebin 584
Ou, Guoyang Zeng, et al. 2023. Predicting emer- 585
gent abilities with infinite resolution evaluation. In 586
The Twelfth International Conference on Learning 587
Representations. 588

Berivan Isik, Natalia Ponomareva, Hussein Hazimeh, 589
Dimitris Paparas, Sergei Vassilvitskii, and Sanmi 590
Koyejo. 2024. Scaling laws for downstream task per- 591
formance of large language models. arXiv preprint 592
arXiv:2402.04177. 593

Leonard Kaufman and Peter J Rousseeuw. 2009. 594
Finding groups in data: an introduction to cluster 595
analysis. John Wiley & Sons. 596

Yifan Li, Yifan Du, Kun Zhou, Jinpeng Wang, 597
Wayne Xin Zhao, and Ji-Rong Wen. 2023. Evalu- 598
ating object hallucination in large vision-language 599
models. arXiv preprint arXiv:2305.10355. 600

Percy Liang, Rishi Bommasani, Tony Lee, Dimitris 601
Tsipras, Dilara Soylu, Michihiro Yasunaga, Yian 602
Zhang, Deepak Narayanan, Yuhuai Wu, Ananya Ku- 603
mar, et al. 2022. Holistic evaluation of language 604
models. arXiv preprint arXiv:2211.09110. 605

Aman Mehra, Rahul Saxena, Taeyoun Kim, Christina 606
Baek, Zico Kolter, and Aditi Raghunathan. 2024. 607
Predicting the performance of foundation mod- 608
els via agreement-on-the-line. arXiv preprint 609
arXiv:2404.01542. 610

John P Miller, Rohan Taori, Aditi Raghunathan, Sh- 611
iori Sagawa, Pang Wei Koh, Vaishaal Shankar, Percy 612
Liang, Yair Carmon, and Ludwig Schmidt. 2021. 613
Accuracy on the line: on the strong correlation be- 614
tween out-of-distribution and in-distribution gener- 615
alization. In International conference on machine 616
learning, pages 7721–7735. PMLR. 617

Long Ouyang, Jeffrey Wu, Xu Jiang, Diogo Almeida, 618
Carroll L. Wainwright, Pamela Mishkin, Chong 619
Zhang, Sandhini Agarwal, Katarina Slama, Alex 620
Ray, John Schulman, Jacob Hilton, Fraser Kelton, 621
Luke Miller, Maddie Simens, Amanda Askell, Peter 622
Welinder, Paul F. Christiano, Jan Leike, and Ryan 623
Lowe. 2022. Training language models to follow 624
instructions with human feedback. In Advances in 625
Neural Information Processing Systems 35: Annual 626
Conference on Neural Information Processing 627
Systems 2022, NeurIPS 2022, New Orleans, LA, 628
USA, November 28 - December 9, 2022. 629

Lorenzo Pacchiardi, Lucy G Cheke, and José 630
Hernández-Orallo. 2024. 100 instances is all you 631
need: predicting the success of a new llm on unseen 632
data by testing on a few instances. arXiv preprint 633
arXiv:2409.03563. 634

635	Yotam Perlitz, Elron Bandel, Ariel Gera, Ofir Arviv,	Laurens Van der Maaten and Geoffrey Hinton. 2008.	691
636	Liat Ein-Dor, Eyal Shnarch, Noam Slonim, Michal	Visualizing data using t-sne. <u>Journal of machine</u>	692
637	Shmueli-Scheuer, and Leshem Choshen. 2023. Ef-	<u>learning research</u> , 9(11).	693
638	cient benchmarking (of language models). <u>arXiv</u>		
639	preprint arXiv:2308.11696.		
640	Felipe Maia Polo, Lucas Weber, Leshem Choshen,	Rajan Vivek, Kawin Ethayarajh, Diyi Yang, and Douwe	694
641	Yuekai Sun, Gongjun Xu, and Mikhail Yurochkin.	Kiela. 2024. <u>Anchor points: Benchmarking mod-</u>	695
642	2024. <u>tinybenchmarks: evaluating llms with fewer</u>	<u>els with much fewer examples</u> . In <u>Proceedings of</u>	696
643	<u>examples</u> . In <u>Forty-first International Conference</u>	<u>of the 18th Conference of the European Chapter of the</u>	697
644	<u>on Machine Learning, ICML 2024, Vienna, Austria,</u>	<u>Association for Computational Linguistics, EACL</u>	698
645	<u>July 21-27, 2024</u> . OpenReview.net.	<u>2024 - Volume 1: Long Papers, St. Julian's, Malta,</u>	699
		<u>March 17-22, 2024</u> , pages 1576–1601. Association	700
		for Computational Linguistics.	701
646	Ameya Prabhu, Vishaal Udandarao, Philip Torr,	Cong Xu, Gayathri Saranathan, Mahammad Parwez	702
647	Matthias Bethge, Adel Bibi, and Samuel Albanie.	Alam, Arpit Shah, James Lim, Soon Yee Wong,	703
648	2024. Lifelong benchmarks: Efficient model eval-	Foltin Martin, and Suparna Bhattacharya. 2024. Data	704
649	uation in an era of rapid progress. <u>arXiv preprint</u>	efficient evaluation of large language models and	705
650	<u>arXiv:2402.19472</u> .	text-to-image models via adaptive sampling. <u>arXiv</u>	706
		preprint arXiv:2406.15527.	707
651	Joseph Lee Rodgers and W. Alan Nicewander. 1988.	Rowan Zellers, Ari Holtzman, Yonatan Bisk, Ali	708
652	<u>Thirteen ways to look at the correlation coefficient</u> .	Farhadi, and Yejin Choi. 2019. Hellaswag: Can a	709
653	<u>The American Statistician</u> , 42(1):59–66.	machine really finish your sentence? <u>arXiv preprint</u>	710
		<u>arXiv:1905.07830</u> .	711
654	Yangjun Ruan, Chris J Maddison, and Tatsunori	Qiyuan Zhang, Fuyuan Lyu, Xue Liu, and Chen Ma.	712
655	Hashimoto. 2024. Observational scaling laws and	2024. Collaborative performance prediction for large	713
656	the predictability of language model performance.	language models. <u>arXiv preprint arXiv:2407.01300</u> .	714
657	<u>arXiv preprint arXiv:2405.10938</u> .		
658	Keisuke Sakaguchi, Ronan Le Bras, Chandra Bhaga-		
659	vatula, and Yejin Choi. 2021. Winogrande: An		
660	adversarial winograd schema challenge at scale.		
661	<u>Communications of the ACM</u> , 64(9):99–106.		
662	Rohan Taori, Achal Dave, Vaishaal Shankar, Nicholas		
663	Carlini, Benjamin Recht, and Ludwig Schmidt.		
664	2020. Measuring robustness to natural distribution		
665	shifts in image classification. <u>Advances in Neural</u>		
666	<u>Information Processing Systems</u> , 33:18583–18599.		
667	Hugo Touvron, Louis Martin, Kevin Stone, Peter Al-		
668	bert, Amjad Almahairi, Yasmine Babaei, Nikolay		
669	Bashlykov, Soumya Batra, Prajjwal Bhargava, Shruti		
670	Bhosale, Dan Bikel, Lukas Blecher, Cristian Canton-		
671	Ferrer, Moya Chen, Guillem Cucurull, David Es-		
672	ioibu, Jude Fernandes, Jeremy Fu, Wenyin Fu, Brian		
673	Fuller, Cynthia Gao, Vedanuj Goswami, Naman		
674	Goyal, Anthony Hartshorn, Saghar Hosseini, Rui		
675	Hou, Hakan Inan, Marcin Kardas, Viktor Kerkez,		
676	Madian Khabsa, Isabel Kloumann, Artem Korenev,		
677	Punit Singh Koura, Marie-Anne Lachaux, Thibaut		
678	Lavril, Jenya Lee, Diana Liskovich, Yinghai Lu, Yun-		
679	ing Mao, Xavier Martinet, Todor Mihaylov, Pushkar		
680	Mishra, Igor Molybog, Yixin Nie, Andrew Poul-		
681	ton, Jeremy Reizenstein, Rashi Rungta, Kalyan		
682	Saladi, Alan Schelten, Ruan Silva, Eric Michael		
683	Smith, Ranjan Subramanian, Xiaoqing Ellen Tan,		
684	Binh Tang, Ross Taylor, Adina Williams, Jian Xiang		
685	Kuan, Puxin Xu, Zheng Yan, Iliyan Zarov, Yuchen		
686	Zhang, Angela Fan, Melanie Kambadur, Sharan		
687	Narang, Aurélien Rodriguez, Robert Stojnic, Sergey		
688	Edunov, and Thomas Scialom. 2023. <u>Llama 2:</u>		
689	<u>Open foundation and fine-tuned chat models</u> . <u>CoRR</u> ,		
690	abs/2307.09288.		

A Related Works

Models Correlation in Predictive Consistency:

Prior works (Taori et al., 2020; Miller et al., 2021; Awadalla et al., 2022) have demonstrated a certain level of correlation between in-distribution (ID) and out-of-distribution (OOD) performances across diverse models and tasks. Building on this foundation, (Baek et al., 2022) and (Mehra et al., 2024) advance this relationship by showing the phenomenon that the agreement between two models on ID data is linearly correlated with their agreement on OOD data, where the accuracy holds the similar linear relationship, enabling accurate estimation of model’s OOD accuracy based solely on ID data. Our work extends this phenomenon to address the challenge of benchmark compression, enabling the selection of more representative subsets for benchmarks.

Coreset Selection for Efficient Benchmarking:

As LLMs proliferate and version updates accelerate, the cost of thoroughly evaluating each model across all benchmarks has become prohibitive, leading to methods that subsample the most representative subsets from each benchmark for more efficient evaluation. (Vivek et al., 2024) clusters examples directly using the confidence scores provided by source models, leveraging these scores to select an optimal subset. Similarly, (Polo et al., 2024) employs an Item Response Theory (IRT) model, trained on the success matrix of each source model across various examples, to derive the latent representations of examples for clustering. (Pacchiardi et al., 2024) introduces a generic assessor framework that predicts the performance of a new LLM on unseen instances using its results on a small reference set, achieving comparable accuracy to full-scale evaluations. (Perlitz et al., 2023) proposes Flash-HELM, which dynamically adjusts the sizes of randomly selected subsets based on model ranking, where higher-ranked models are evaluated with greater precision. (Prabhu et al., 2024) proposes the Sort & Search (S&S) strategy, which leverages the difficulties of examples and dynamic programming to select the coreset. (Xu et al., 2024) synthesizes several methods and dynamically chooses the optimal subset selection method for each benchmark but requires many examples to determine the best approach. Despite these advancements, these methods often struggle with substantial distribution shifts between the source and target models, caused by the discrepancy

between their predictive consistency, potentially causing significant distortion in estimating the target model’s performance. Extending the approach of (Vivek et al., 2024), our work alleviates this issue by dynamically selecting a native source model set with the highest prediction consistency to the target model, ensuring the selection of a tailored coreset for each target model that best represents the benchmark.

Scaling Approaches for Model Performance

Estimations: Scaling law describes the relationship between model properties (e.g., FLOPs used during training, model parameter size) and model capabilities. Recent works (Hu et al., 2023; Ruan et al., 2024; Isik et al., 2024) have leveraged scaling laws to predict model performance on various downstream tasks, reducing the computational cost of evaluating models on complex downstream tasks. (Zhang et al., 2024) simplifies those approaches by utilizing the relationships between model families and their collaborative overall performance across tasks rather than fitting scaling laws. The aforementioned methods typically rely on overall model performance across several benchmarks and specific design factors (e.g., model size or training data properties) to either fit scaling curves or investigate correlations between models on various tasks. In contrast, our approach addresses a more general case by reducing the evaluation cost for multiple models on a single benchmark, offering a more efficient performance estimation framework.

B More Experimental Results

B.1 Comprehensive Experimental Results Across All Datasets

In Table 6, we present a comprehensive comparison of our approach against all baseline methods across the full range of benchmark datasets. The results indicate that our method consistently outperforms every baseline under all considered inference counts, thereby demonstrating the overall effectiveness of our proposed approach.

B.2 Detailed Calibration Ablation Results

Table 7 presents the results of our ablation study, comparing our TAILOREDBENCH method with and without the calibrated performance estimation process under 30 inference counts. The calibrated version of our method generally achieves higher Kendall’s τ scores and lower mean absolute errors

Benchmarks	Inference counts	20		25		30		35		40	
		$\tau \uparrow$	MAE \downarrow	$\tau \uparrow$	MAE \downarrow	$\tau \uparrow$	MAE \downarrow	$\tau \uparrow$	MAE \downarrow	$\tau \uparrow$	MAE \downarrow
ARC Challenge	RANDOM	0.626	0.078	0.659	0.065	0.676	0.067	0.694	0.062	0.712	0.057
	ANCHORPOINTS	<u>0.662</u>	0.064	<u>0.663</u>	0.058	<u>0.676</u>	0.053	<u>0.713</u>	0.048	<u>0.714</u>	0.043
	GP-IRT	0.589	<u>0.046</u>	0.620	<u>0.046</u>	0.662	<u>0.036</u>	0.681	<u>0.036</u>	0.695	<u>0.029</u>
	TAILOREDBENCH	0.711	0.031	0.737	0.029	0.756	0.028	0.766	0.027	0.773	0.027
Hellaswag	RANDOM	0.811	0.083	0.836	0.077	0.850	0.066	0.863	0.060	0.871	0.058
	ANCHORPOINTS	<u>0.860</u>	<u>0.060</u>	<u>0.880</u>	0.061	<u>0.877</u>	0.067	<u>0.897</u>	0.059	<u>0.898</u>	0.057
	GP-IRT	0.724	0.062	0.776	<u>0.053</u>	0.810	<u>0.043</u>	0.827	<u>0.038</u>	0.849	<u>0.032</u>
	TAILOREDBENCH	0.900	0.020	0.909	0.018	0.913	0.018	0.914	0.017	0.918	0.017
GSM8K	RANDOM	<u>0.811</u>	0.062	<u>0.828</u>	0.055	<u>0.839</u>	0.052	<u>0.847</u>	0.049	<u>0.858</u>	0.044
	ANCHORPOINTS	0.786	0.087	0.791	0.079	0.796	0.073	0.800	0.071	0.799	0.071
	GP-IRT	0.787	<u>0.055</u>	0.807	<u>0.047</u>	0.829	<u>0.041</u>	0.842	<u>0.038</u>	0.858	<u>0.034</u>
	TAILOREDBENCH	0.852	0.035	0.858	0.034	0.863	0.033	0.869	0.031	0.878	0.029
Winogrande	RANDOM	0.373	0.078	0.408	0.067	0.446	0.062	0.470	0.055	0.492	0.052
	ANCHORPOINTS	<u>0.472</u>	0.086	<u>0.487</u>	0.085	<u>0.514</u>	0.075	<u>0.521</u>	0.087	<u>0.518</u>	0.073
	GP-IRT	0.263	<u>0.041</u>	0.313	<u>0.038</u>	0.353	<u>0.038</u>	0.392	<u>0.036</u>	0.419	<u>0.034</u>
	TAILOREDBENCH	0.565	0.028	0.568	0.026	0.604	0.024	0.608	0.023	0.618	0.022
POPE	RANDOM	<u>0.488</u>	0.058	<u>0.510</u>	0.054	0.507	0.048	0.515	0.044	0.547	0.040
	ANCHORPOINTS	0.474	0.040	0.483	0.038	<u>0.518</u>	<u>0.034</u>	<u>0.547</u>	<u>0.033</u>	<u>0.556</u>	0.031
	GP-IRT	0.481	<u>0.038</u>	0.470	<u>0.037</u>	0.462	0.036	0.482	0.034	0.477	0.033
	TAILOREDBENCH	0.521	0.036	0.547	0.035	0.562	0.031	0.563	0.031	0.574	<u>0.032</u>

Table 6: Results on all benchmarks. Values in bold represent the best results, while values that are underlined represent the second-best results.

(MAE) across various benchmarks and inference counts, demonstrating that the calibrated performance estimation process effectively enhances the performance estimation ability of our method.

B.3 Preference for Intra-Family Native Source Models

We conducted an additional analysis on the GSM8K dataset to investigate whether models within the same family (e.g., Llama, Mistral) tend to select their own family members as native source models. As shown in Table 8, with a similar number of models from each family within the source and target model set, the results indicate a significant intra-family preference. On average, each llama-series model selected approximately 5.3 Mistral models and 7.0 Llama models as their native source models. Similarly, each Mistral-series model chose about 6.7 Mistral models and 3.7 Llama models on average. These findings suggest that models exhibit a bias toward source models with similar architectures, potentially due to shared representation spaces or analogous decision boundaries. This intra-family affinity may facilitate more accurate performance estimation, as the selected native source models can better capture the nuances and prediction patterns distinctive to their

respective model lineages.

B.4 Comprehensive G-set Size Evaluation Across Benchmarks

In this section, we present a comprehensive evaluation of how varying G-set sizes affect our method’s performance across multiple benchmarks. Table 9 reports Kendall’s τ and MAE metrics for G-set sizes ranging from 5 to 25 for each benchmark. These results provide deeper insights into selecting the optimal G-set size and support the conclusions drawn in the main text.

B.5 Comprehensive Distance Measures Ablation Across Benchmarks

Here, we provide comprehensive results of our ablation study evaluating the impact of different distance measures on our method’s performance with 30 inference counts across various benchmarks. Table 10 presents detailed Kendall’s τ and MAE metrics for cosine similarity, Manhattan distance, and correlation distance across all datasets. These results offer deeper insights into the effectiveness of Element-Wise Distance measures in enhancing benchmark compression.

Distance	ARC Challenge		Hellaswag		GSM8K		Winogrande		POPE	
	$\tau \uparrow$	MAE \downarrow	$\tau \uparrow$	MAE \downarrow	$\tau \uparrow$	MAE \downarrow	$\tau \uparrow$	MAE \downarrow	$\tau \uparrow$	MAE \downarrow
NON-CALIBRATED	0.748	0.026	0.910	0.017	0.862	0.036	0.588	0.028	0.531	0.043
CALIBRATED	0.756	0.028	0.913	0.018	0.863	0.033	0.604	0.024	0.562	0.031

Table 7: Detailed ablation results for calibrated performance estimation process across all benchmarks.

Model Family	Avg. Selected Mistral Models	Avg. Selected Llama Models
Llama	5.3	7.0
Mistral	6.7	3.7

Table 8: Statistics of native source model selection within model families on GSM8K benchmark.

B.6 Demonstration of Method Effectiveness with Variance

In this section, we present visual comparisons of our method and other approaches, including their respective variances, as illustrated in Figures 5 to 9. The results demonstrate that our method outperforms the baseline methods on all datasets and exhibits greater robustness (with smaller variance).

B.7 More Analyses On the Impact of Native Source Model Quantity on Our Method

In this section, we maintain the overall prediction consistency between the native source models and the target models constant, while varying the proportion of the source models designated as native source models from 20% to 100% for the target models across various benchmarks. The results are illustrated in Figures 10 to 14, indicating that, under the condition of maintaining the prediction consistency between the native source models and the target model, the number of native source models significantly influences the method’s performance.

B.8 More Analyses On the Impact of Native Source Models’ Prediction Consistency on Our Method

We conduct ablation studies by selecting native source models based on their prediction consistency with the target model across various benchmarks, ranging from the top 20% to the 80%~100% range. The results, presented in Figures 15 to 19, indicate that the performance of the method significantly declines as the prediction consistency between the native source models and the target model decreases, under the condition of keeping

the number of native source models constant.

B.9 Extended Results on Optimal Native Source Model Selection

This section presents the results of our method as the number of native source models is incrementally increased based on their prediction consistency with the target model. The results in Figures 20 to 23 show that, overall, Kendall’s τ initially increases and then decreases as the number of native source models increases, while the MAE initially decreases and then increases with the increase in the number of native source models.

Moreover, Our method adaptively selects 45 native source models for the ARC Challenge benchmark, 40 for the Hellaswag benchmark, 33 for the Winogrande benchmark, and 35 for the POPE benchmark. These selections represent near-optimal numbers of native source models, as demonstrated in Figures 20 to 23.

C Models Used in Our Experiments

Tables 11, 12, 13, 14 provide comprehensive lists of models corresponding to each benchmark.

G-set	ARC Challenge		Hellaswag		GSM8K		Winogrande		POPE	
	$\tau \uparrow$	MAE \downarrow	$\tau \uparrow$	MAE \downarrow	$\tau \uparrow$	MAE \downarrow	$\tau \uparrow$	MAE \downarrow	$\tau \uparrow$	MAE \downarrow
5	0.719	0.031	0.912	0.019	0.865	0.035	0.624	0.026	0.549	0.037
10	0.756	0.028	0.913	0.018	0.863	0.033	0.604	0.024	0.562	0.031
15	0.751	0.029	0.911	0.018	0.854	0.034	0.608	0.025	0.556	0.033
20	0.740	0.029	0.910	0.018	0.862	0.034	0.621	0.026	0.541	0.034
25	0.725	0.030	0.909	0.019	0.851	0.036	0.638	0.026	0.533	0.036

Table 9: Detailed results for G-set size across all benchmarks.

Distance	ARC Challenge		Hellaswag		GSM8K		Winogrande		POPE	
	$\tau \uparrow$	MAE \downarrow	$\tau \uparrow$	MAE \downarrow	$\tau \uparrow$	MAE \downarrow	$\tau \uparrow$	MAE \downarrow	$\tau \uparrow$	MAE \downarrow
CORRELATION	0.766	0.033	0.903	0.019	0.828	0.041	0.557	0.029	0.547	0.038
COSINE	0.746	0.031	0.914	0.019	0.827	0.040	0.616	0.024	0.577	0.024
MANHATTAN	0.756	0.028	0.913	0.018	0.863	0.033	0.604	0.024	0.562	0.031

Table 10: Detailed ablation results for distance selection across all benchmarks.

Benchmark	Model Names
ARC Challenge	Qwen2-72B-Instruct, Meta-Llama-3-70B-Instruct, Qwen2-72B, zephyr-orpo-141b-A35b-v0.1, Phi-3-medium-4k-instruct, Yi-1.5-34B-Chat, c4ai-command-r-plus, Qwen1.5-110B, Smaug-72B-v0.1, Qwen1.5-110B-Chat, Yi-1.5-9B-Chat, Qwen1.5-32B-Chat, Nous-Hermes-2-Mixtral-8x7B-DPO, deepseek-llm-67b-chat, Qwen1.5-32B, Yi-1.5-34B-32K, Meta-Llama-3-70B, Phi-3-mini-4k-instruct, mixtral-8x22B-v0.3, Mixtral-8x22B-v0.1, Phi-3-mini-128k-instruct, Yi-1.5-34B, c4ai-command-r-v01, Qwen2-7B-Instruct, Hermes-2-Theta-Llama-3-8B, aya-23-35B, Mixtral-8x7B-Instruct-v0.1, notux-8x7b-v1, Meta-Llama-3-8B-Instruct, Yi-34B-Chat, Smaug-34B-v0.1, Qwen2-7B, Nous-Hermes-2-SOLAR-10.7B, K2-Chat, Yi-1.5-9B-Chat-16K, Llama-3-Refueled, WizardLM-70B-V1.0, Yi-34B, Yi-1.5-6B-Chat, NeuralDaredevil-8B-abliterated, Yi-1.5-9B, Nous-Hermes-2-Mixtral-8x7B-SFT, Hermes-2-Pro-Mistral-7B, Hermes-2-Pro-Llama-3-8B, openchat_3.5, neural-chat-7b-v3-2, OpenHermes-2-Mistral-7B, OpenHermes-2.5-Mistral-7B, Qwen1.5-14B-Chat, Nous-Hermes-2-Mistral-7B-DPO, neural-chat-7b-v3-1, Starling-LM-7B-alpha, Qwen1.5-14B, neural-chat-7b-v3-3, Yi-34B-200K, SOLAR-10.7B-Instruct-v1.0, Yi-1.5-9B-32K, Mixtral-8x7B-v0.1, Mistral-7B-Instruct-v0.3, zephyr-7b-alpha, Mistral-7B-Instruct-v0.2, dolphin-2.9-llama3-8b, Llama-2-70b-hf, Orca-2-13b, Llama-3-8B-Instruct-Gradient-1048k, neural-chat-7b-v3, zephyr-7b-beta, Mistral-7B-OpenOrca, Yi-9B, Yi-9B-200K, DeciLM-7B-instruct, gemma-1.1-7b-it, SOLAR-10.7B-v1.0, merlinite-7b, Qwen1.5-7B-Chat, 14B, Yi-1.5-6B, stablelm-2-12b-chat, aya-23-8B, zephyr-7b-gemma-v0.1, Yarn-Solar-10b-32k, phi-2, phixtral-2x2_8, gemma-7b, Qwen1.5-7B, WizardLM-13B-V1.2, LLaMA-Pro-8B-Instruct, Yarn-Solar-10b-64k, DeciLM-7B, OrpoLlama-3-8B, Qwen1.5-MoE-A2.7B-Chat, deepseek-llm-7b-chat, Mistral-7B-v0.1, CollectiveCognition-v1.1-Mistral-7B, Mistral_Pro_8B_v0.1, Mistral-7B-v0.3, Orca-2-7b, Mistral-7B-v0.2, Yi-6B-Chat, Qwen2-1.5B-Instruct, stablelm-2-12b, openchat_v3.2, falcon-11B, Yi-6B, Mistral-7B-Instruct-v0.1, Yarn-Mistral-7b-64k, Meta-Llama-3-8B, Yarn-Mistral-7b-128k, gemma-7b-it, openchat_v3.2_super, Llama-2-70b-chat-hf, Qwen1.5-MoE-A2.7B, stablelm-zephyr-3b, Qwen1.5-4B-Chat, starcoder2-15b, OpenHermes-13B, MetaMath-Mistral-Pro, Yi-6B-200K, falcon-40b, Qwen1.5-4B, Llama-2-13b-chat-hf, Llama-2-13b-hf, vicuna-7b-v1.5, OLMo-7B-Instruct-hf, internlm2-chat-1_8b, falcon-40b-instruct, Qwen2-1.5B, deepseek-moe-16b-chat, OpenHermes-7B, Llama-2-7b-chat-hf, Nous-Hermes-llama-2-7b, stablelm-2-zephyr-1_6b, Qwen1.5-1.8B, Qwen1.5-1.8B-Chat, LLaMA-Pro-8B, Llama-2-7b-hf, stablelm-2-1_6b-chat, internlm2-1_8b, Yarn-Llama-2-13b-128k, NexusRaven-V2-13B, starcoder2-7b, Llama-2-7B-32K-Instruct, deepseek-llm-7b-base, recurrentgemma-2b-it, gemma-1.1-2b-it, granite-7b-base, deepseek-moe-16b-base, gemma-2b, stablelm-3b-4e1t, gemma-2b-it, Yarn-Llama-2-7b-64k, Qwen2-0.5B, phi-1_5

Table 11: Models used for ARC Challenge benchmark.

Benchmark	Model Names
HellaSwag	LLaMAntino-3-ANITA-8B-Inst-DPO-ITA, luxia-21.4b-alignment-v1.0, UNA-ThePitbull-21.4-v1, T3Q-ko-solar-dpo-v6.0, MultiVerse_70B, RoleBeagle-11B, Capricorn-7B-DPO, Tess-2.0-Llama-3-70B, Truthful_DPO_MOE_19B, multimaster-7b-v5, guanaco-65B-HF, Fusion-Net_34Bx2_MoE_v0.1, Mixtral-8x7B-v0.1, Evangelion-7B, Lumina-5.5-Instruct, Mistral-Hermes-2x7b, Bagel-Hermes-2x34B, shqiponja-15b-v1, CollectiveCognition-v1.1-Mistral-7B-dare-0.85, etri-ones-solar, mpt-30b-instruct, openbuddy-mixtral-7bx8-v18.1-32k, bagel-dpo-7b-v0.4, OpenHermes-2.5-Mistral-7B, NeuralHermes-2.5-Mistral-7B, dolphin-2.1-mistral-7b-snr-math-laser, NeuralHermes-2.5-Mistral-7B, openbuddy-qwen1.5-32b-v21.1-32k, internlm2-20b-llama, Matter-0.2-7B-DPO, aioboros-13b-gpt4-1.2, L3-SnowStorm-v1.15-4x8B-B, Pallas-0.5-LASER-0.6, BgGPT-7B-Instruct-v0.1, Seagull-llama-3-8B-orpo-v0.5, vigogne-7b-instruct, Llama-2-7b-chat-hf-activity-fine-tuned-v4, Llama-2-7b-chat-hf-activity-fine-tuned-v3, vicuna-class-tutor-7b-ep3, Llama-2-7b-chat-hf-afr-200step-flan-v2, llama3-8b-instruct-align-test1-kto, MFANN3bv0.7, openbuddy-yi1.5-9b-v21.1-32k, openbuddy-mixtral-7bx8-v17.1-32k, odia_llama2_7B_base, MT7Bi-alpha-dpo-v0.2, llama-shishya-7b-ep3-v2, Instruct_Yi-6B_Dolly15K, Gaja-v2.00-dpo, phi-2-OpenHermes-2.5, lion-gemma-7b-cn-v2, ToRoLaMa-7b-v1.0, gogpt-7b, Amber, open_llama_3b_v2, openllama_3b_EvolInstruct_lora_merged, gemma-7B-it-firefly, Qwen1.5-4B, google-gemma-7b-it-dpo-v1, openhermes-2b-gemma-sft-qlora, RedPajama-INCITE-Chat-3B-v1, mistral_v1, gpt-j-6b, GPT-J-Pyg_PPO-6B, ScarletPajama-3B-HF, LLama2-7B-Structural-Prune-1.5x, illuni-llama-2-ko-7b-test, RedPajama-INCITE-Chat-3B-ShareGPT-11K, RedPajama-INCITE-Base-3B-v1, Guanaco-3B-Uncensored-v2-GPTQ, glaive-coder-7b, xglm-7.5B, gpt-sw3-6.7b, cisco-iNAM-1.1B, pythia-2.7b, qd-phi-1.5, pythia-2.8b-deduped, LLMRa-2.7B, Tinyllama-1.3B-Cinder-Reason-Test-2, TinyPoliticalLlama-1.1B, Galpaca-30b-MiniOrca, finetune_test_qwen15-1-8b-sft-lora, TinyLlama-1.1B-Chat-v0.3, TinyLlama-1.1B-Chat-v0.1, CroissantLLMBase, pygmalion-2.7b, blossom-v2-3b, falcon_1b_stage3, MiniMerlin-3b-v0.1, DPO-miniguanaco-1.5T, CodeQwen1.5-7B-Chat, yayi2-30b-llama, rho-math-1b-v0.1, LLMRa-1.3B_V2, TinyLlama-1.1B-intermediate-step-480k-1T, gemma-2b-ko-dev-pbmt192, gpt2-chatbot, CodeLlama-7b-Python-hf, Deita-500m, TinyWand-SFT, tinyllama-coder-py-v13, d-Qwen1.5-1.8B, TinyLlama-1.1B-intermediate-step-240k-503b, dlite-v1-1_5b, pythia-1b-deduped, gpt2-large, WizardCoder-Guanaco-15B-V1.0, Qwen1.5-0.5B-vortex-v2, Sailor-0.5B-Chat, WizardCoder-Guanaco-15B-V1.1, Alpaca_refine_gpt2_e1_se0, deepseek-coder-1.3b-chat, speechless-coder-ds-1.3b, Instruct_GPT, deepseek-coder-1.3b-chat-and-function-calling, megatron-gpt2-345m, starcoderbase-3b, dlite-v1-355m, gov-qna-ko-merged, SSH_355M, CodeLlama-34b-Instruct-hf, CodeLlama-34B-Instruct-fp16, mptk-1b, KoAlpaca-Polyglot-5.8B, Llama-160M-Chat-v1, llama-160m, CodeLlama-34b-hf, KoAlpaca-KoRWKV-6B, Quokka_590m, pruned-yi-3b-prerelease-ckpt01, gpt2_test, finetuned-gpt2-tiny, Kaori-34b-v2, kaori-34b-v4, tiny_starcoder_py, GPT-2-Large-51k-steps, DialogGPT-small, test_mistral2, pythia-31m-KI_v1-2048-scratch

Table 12: Models used for Hellaswag benchmark.

Benchmark	Model Names
GSM8K & Winogrande	ExtremeDolphin-MoE, Mistral-7B-Instruct-v0.2-sparsity-20, PiVoT-SUS-RP, polyglot-math-4x7b, SOLAR-10B-Nector-DPO-Jawade, Starling-LM-11B-alpha, NeuralPipe-7B-slerp, oswald-7b, MistralTrixTest, Sensualize-Mixtral-bf16, Sensualize-Solar-10.7B, FusionNet_passthrough, finance-chat, Kunoichi-7B, dolphin-2.2.1-mistral-7b, CarbonVillain-en-10.7B-v3, xDAN-SlimOrca, Mistral-11B-v0.1, dm7b_sft_gpt88w_merge, Loyal-Macaroni-Maid-7B, Yi-34B-200K-DARE-merge-v5, WinterGoddess-1.4x-70B-L2, vicuna-class-shishya-ac-hal-13b-ep3, Kaori-34B-v1, mistral-megamerge-dare-7b, Chupacabra-8x7B-MoE, bagel-7b-v0.1, Mixtral-8x7B-v0.1, openbuddy-deepseek-67b-v15-base, Falkor-7b, synapsellm-7b-mistral-v0.4-preview3, llama2-13b-ft-openllm-leaderboard-v1, synapsellm-7b-mistral-v0.3-preview, Tess-M-v1.3, monika-ddlc-7b-v1, speechless-mistral-7b-dare-0.85, mistral-7b-v0.1-layla-v1, Mistral-v0.1-PeanutButter-v0.0.2-7B, chronos-70b-v2, L2-7b-Beluga-WVG-Test, llama-2-13b-FINETUNE3_3.3w-r8-gate_up_down, airoboros-c34b-2.2.1, llama-2-13b-FINETUNE4_3.8w-r8-q_k_v_o, llama-2-13b-FINETUNE3_3.3w-r16-gate_up_down, MLewd-Chat-v2-13B, Mistral-7B-v0.1-Open-Platypus, llama-2-13b-FINETUNE1_17w-r4, EverythingLM-13b-V3-peft, Llama2-7B-guanaco-1k, llama-2-13b-FINETUNE4_3.8w-r8-q_k_v_o_gate_up_down, Koss-7B-chat, ReMM-v2.2-L2-13B, WizardLM-1.0-Uncensored-CodeLlama-34b, airoboros-13b, airoboros-7b-gpt4-1.4.1-qlora, Wizard-Vicuna-7B-Uncensored-HF, Luban-Platypus2-13B-QLora-0.80-epoch, CodeLlama-34b-hf, airoboros-33b-gpt4-m2.0, llama2-22b-blocktriangular, GPT-JT-6B-v0, llama2-70b-oasst-sft-v10, vigogne-7b-instruct, based-30b, mpt-30b-chat, qCammel-70x, GiftedConvo13bLoraNoEconsE4, llama-2-13b-platypus-vicuna-wizard, GOAT-7B-Community, genz-13b-v2, chronolima-airo-grad-12-13B, Vicuna-13B-CoT, Llama-2-7b-ft-instruct-es, OpenOrca-Preview1-13B, Tulpar-7b-v0, zephyr-7b-sft-full, Mixtral-Orca-v0.1, Marcoroni-7b-DPO-Merge, Aquila2-34B, SOLAR-10.7B-Instruct-v1.0-128k, dolphin-2.6-mistral-7b-dpo-orca-v3, flux-7b-v0.1, Turdus, A0110, yayi2-30b-llama, NeuralMarcoro14-7B, Deacon-34b-Adapter, test0, Pallas-0.5-LASER-0.4, Marcoro14-7B-ties, Antares-11b-v1, CodegebraGPT-10b, Mistral-Syndicate-7B, Nous-Hermes-2-Yi-34B, Half-NSFW_Noromaid-7b, neural-chat-7b-v3-3-wizardmath-dare-me, apricot-wildflower-20, SauerkrautLM-UNA-SOLAR-Instruct, kalomaze-stuff, Walter-Mistral-7B, Starling-LM-alpha-8x7B-MoE, una-neural-chat-v3-3-P2-OMA, Dans-07YahooAnswers-7b, Chupacabra-7B-v2.03, PlatYi-34B-200K-Q, chinese-alpaca-2-13b-16k, ALMA-7B-Ja-V2, speechless-code-mistral-7b-v2.0, Mistral7B_adaptor_v1, notus-7b-v1, Chupacabra-7B-v2, SciPhi-Self-RAG-Mistral-7B-32k, Ferret-7B, llama-2-13B-instructed, glaive-coder-7b, Mistralic-7B-1, kuchiki-12-7b, llama_7b_lora, Slerpeno, Llama2-7b-openorca-mc-v2-dpo, CAMEL-13B-Role-Playing-Data, starchat-beta, test-model2, Huginn-13b-v1.2, Dans-AdventurousWinds-7b, Wizard-Vicuna-13B-Uncensored-HF, Llama-2-13b-hf-ds_wiki_1024_full_r_64_alpha_16_merged, Emerald-13B, koala-13B-HF, tulu-7B-fp16, airoboros-c34b-2.1, airoboros-7b-gpt4-1.1, 13B-Chimera, Nous-Hermes-Platypus2-13B-QLoRA-0.80-epoch, airoboros-12-7b-gpt4-m2.0, llama-7b, llama-65b-instruct, Flash-Llama-7B, StableBeluga-13B, huginnv1.2, llama_13b_sharegpt94k_fastchat, CAMEL-13B-Combined-Data, MelangeC-70b, chronos-13b-v2, stack-llama-2, CodeLlama-34b-Python-hf, UltraLM-65b, Platypus-30B, bimoGPT-llama2-13b, test-llama2-7b

Table 13: Models used for GSM8K and Winogrande benchmark.

Benchmark	Model Names
POPE	InternVL2-76B, paligemma-3b-mix-448, InternVL-Chat-V1-5, cambrian_13b, cogvlm-chat, CloudWalk, Ovis1.5-Gemma2-9B, cambrian_8b, InternVL2-26B, Ovis1.5-Llama3-8B, llava_next_vicuna_13b, glm-4v-9b, emu2_chat, llava_next_mistral_7b, llava_next_vicuna_7b, WeMM, cambrian_34b, llava_next_llama3, 360VL-70B, Bunny-llama3-8B, GLM4V, MiniCPM-V-2, llava_next_qwen_32b, Yi-Vision, InternVL2-2B, GeminiPro1-5, InternVL2-8B, llava_next_interleave_7b_dpo, XComposer2d5, MiniCPM-V-2_6, Mini-InternVL-Chat-2B-V1-5, cogvlm2-llama3-chat-19B, llava_next_yi_34b, Step1V, InternVL2-1B, InternVL2-4B, Phi-3-Vision, llava_next_interleave_7b, monkey-chat, OmniLMM_12B, InternVL2-40B, idefics2_8b, deepseek_vl_7b, GPT4o_20240806, sharecaptioner, monkey, llava-v1.5-7b-xtuner, GPT4o_HIGH, RekaEdge, GPT4o, Mantis-8B-Idefics2, MiniCPM-Llama3-V-2_5, llava-llama-3-8b, sharegpt4v_7b, Mini-InternVL-Chat-4B-V1-5, llava-internlm-7b, llava-v1.5-13b-xtuner, sharegpt4v_13b, llava_v1.5_7b, GPT4o_MINI, deepseek_vl_1.3b, RekaFlash, llava_v1.5_13b, Mantis-8B-siglip-llama3, MiniCPM-V, QwenVLPlus, Mantis-8B-clip-llama3, Yi_VL_6B, llava-internlm2-20b, XComposer2_1.8b, mPLUG-Owl2, GPT4V, Yi_VL_34B, llava-internlm2-7b, Claude3-5V_Sonnet, MMAIaya, instructblip_7b, XComposer2, XComposer2_POPE_TEST, TransCore_M, Claude3V_Haiku, Claude3V_Sonnet, Claude3V_Opus, idefics_9b_instruct, chameleon_30b, QwenVLMax, qwen_chat, llava_v1_7b, PandaGPT_13B, qwen_base, XComposer, MiniGPT-4-v1-7B, VisualGLM_6b, flamingov2, MiniGPT-4-v2, VXVERSE, idefics_80b_instruct, chameleon_7b, XComposer2_4KHD

Table 14: Models used for POPE benchmark.

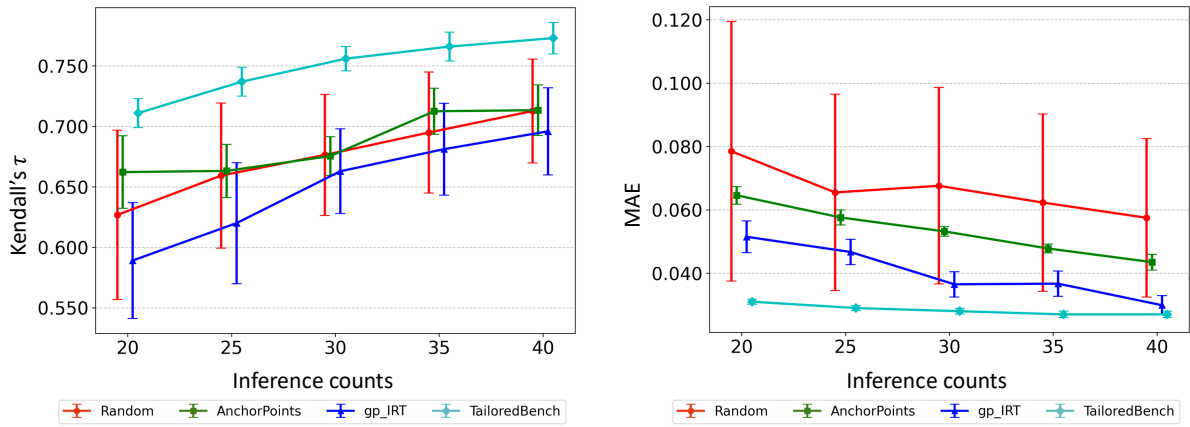


Figure 5: Demonstration of method effectiveness with variance on ARC Challenge benchmark.

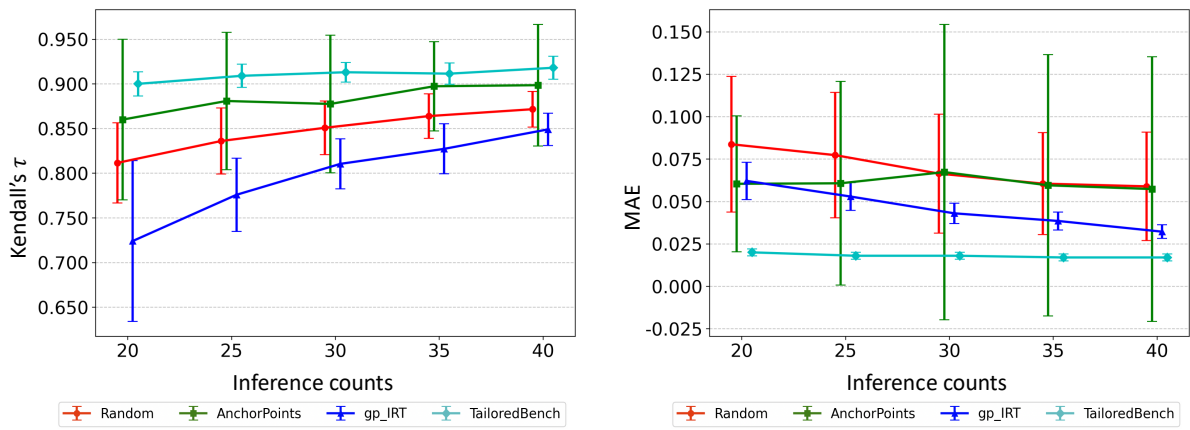


Figure 6: Demonstration of method effectiveness with variance on Hellaswag benchmark.

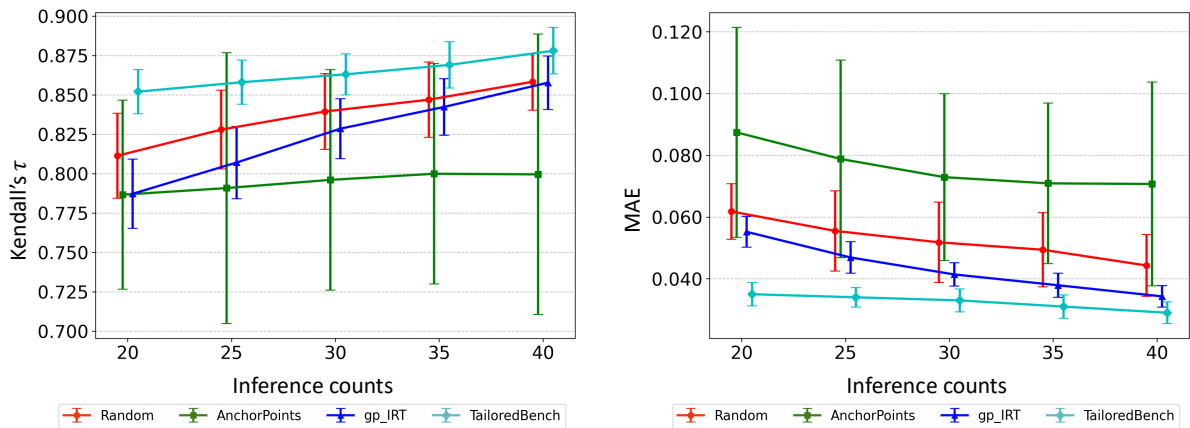


Figure 7: Demonstration of method effectiveness with variance on GSM8K benchmark.

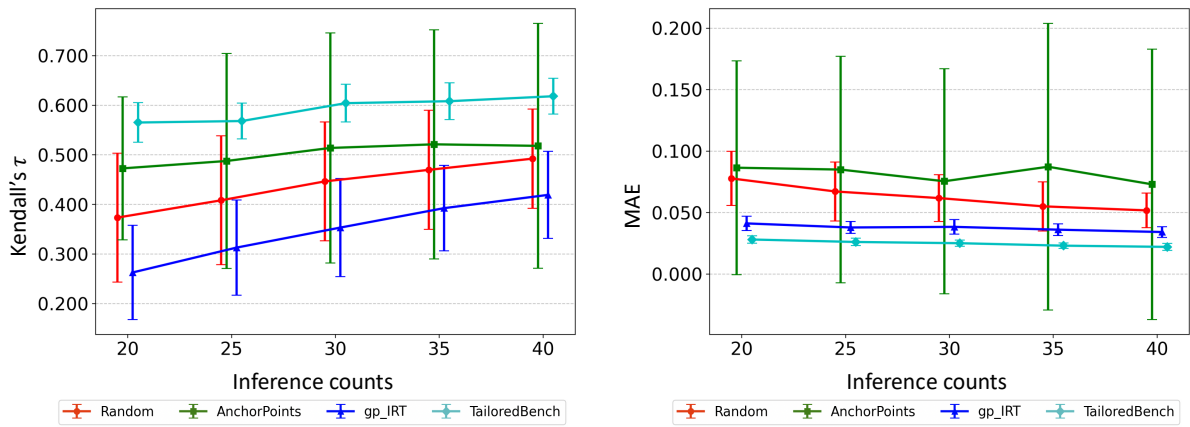


Figure 8: Demonstration of method effectiveness with variance on winogrande benchmark.

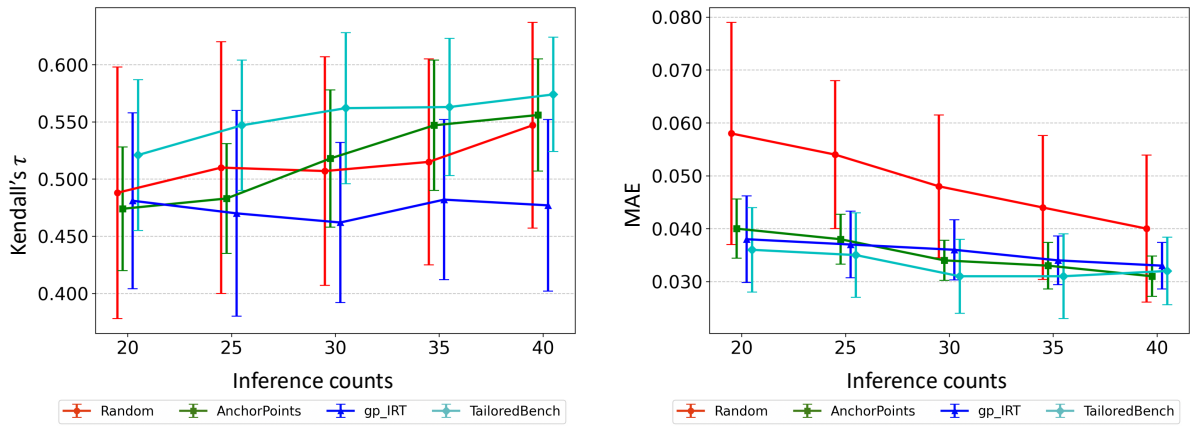


Figure 9: Demonstration of method effectiveness with variance on POPE benchmark.

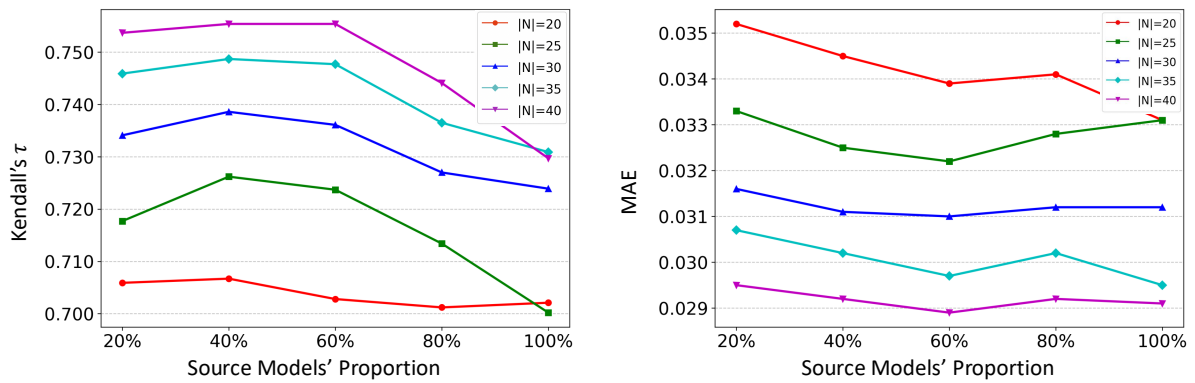


Figure 10: The impact of the quantity of Native Source Models (with prediction consistency kept the same) on ARC Challenge benchmark.

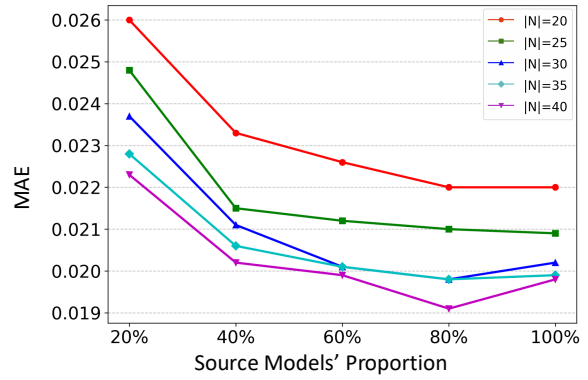
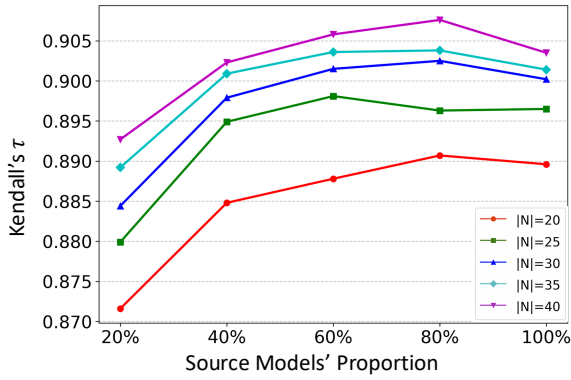


Figure 11: The impact of the quantity of Native Source Models (with prediction consistency kept the same) on Hellaswag benchmark.

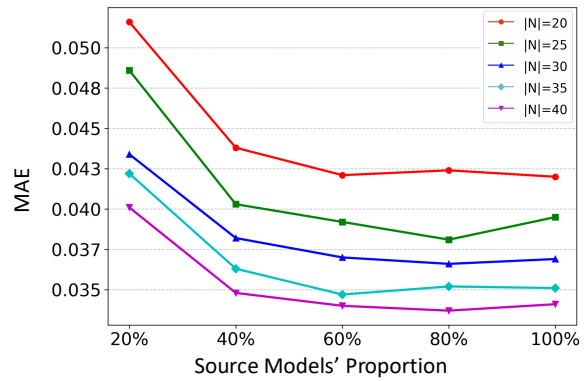
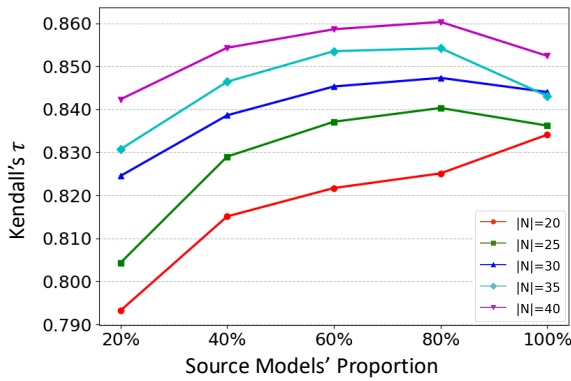


Figure 12: The impact of the quantity of Native Source Models (with prediction consistency kept the same) on GSM8K benchmark.

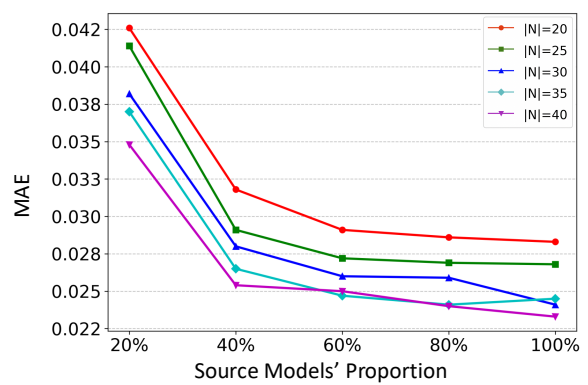
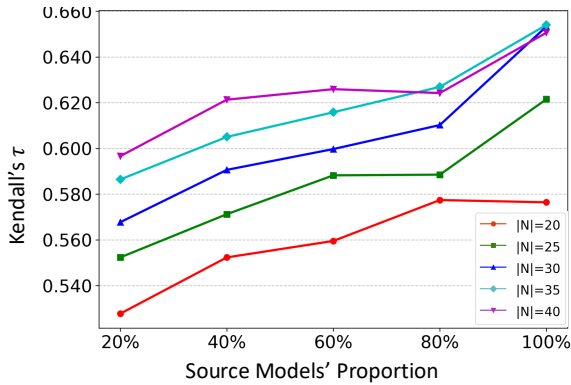


Figure 13: The impact of the quantity of Native Source Models (with prediction consistency kept the same) on Winogrande benchmark.

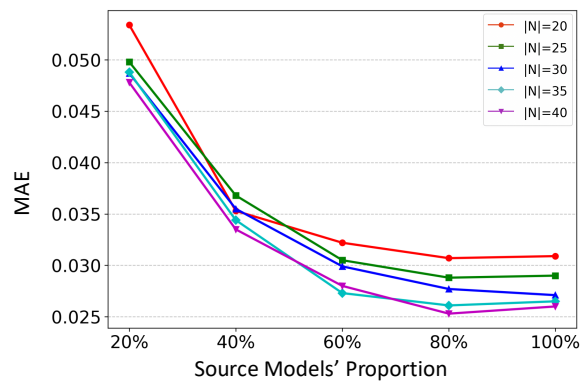
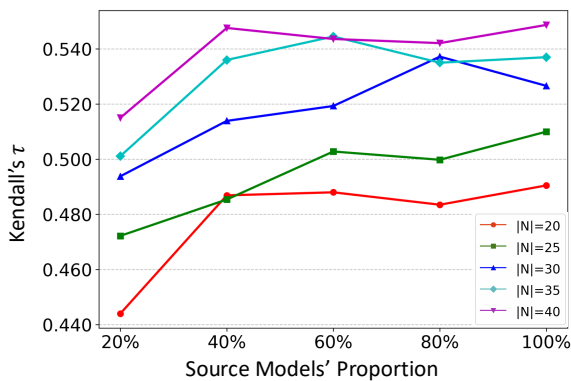


Figure 14: The impact of the quantity of Native Source Models (with prediction consistency kept the same) on POPE benchmark.

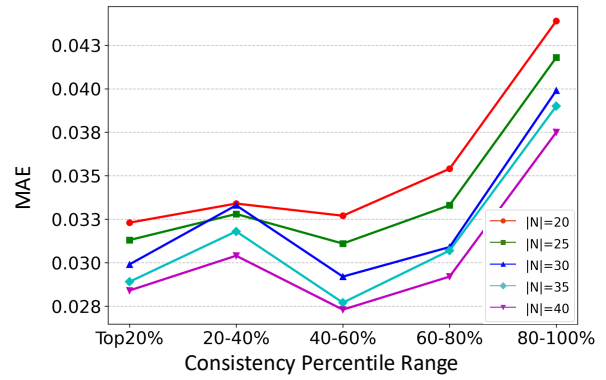
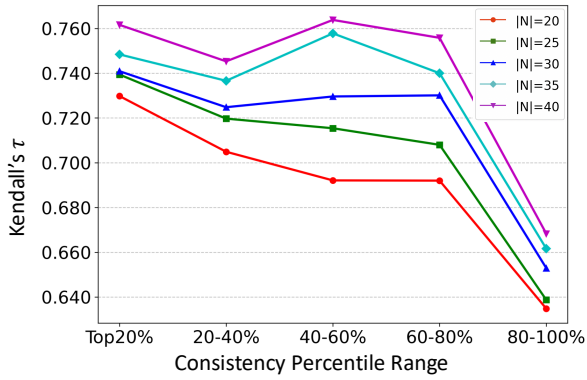


Figure 15: The impact of prediction consistency between the Native Source Model and Target Model (with quantity kept the same) on ARC Challenge benchmark.

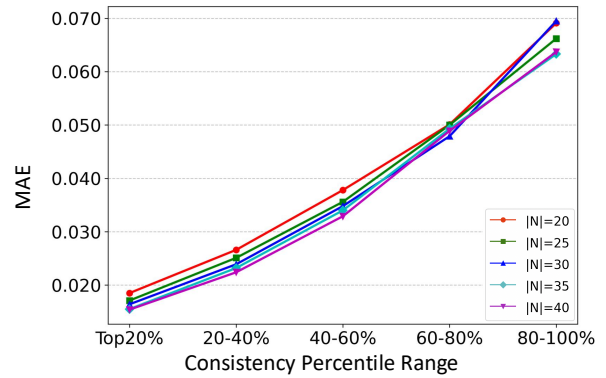
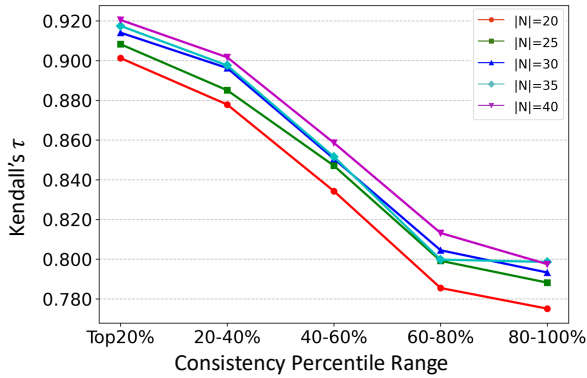


Figure 16: The impact of prediction consistency between the Native Source Model and Target Model (with quantity kept the same) on Hellaswag benchmark.

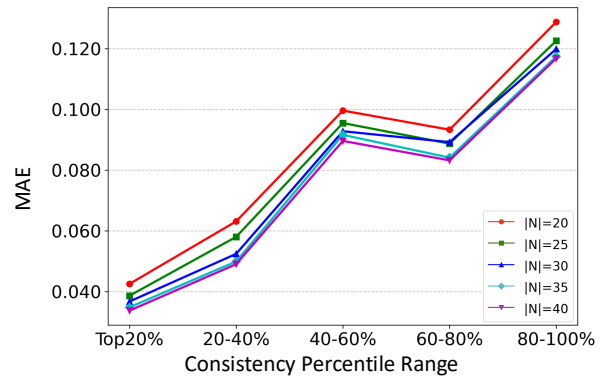
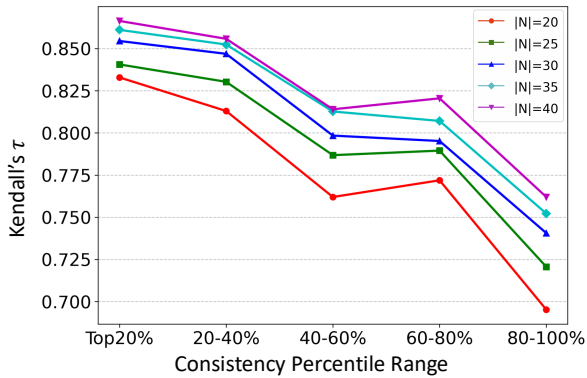


Figure 17: The impact of prediction consistency between the Native Source Model and Target Model (with quantity kept the same) on GSM8K benchmark.

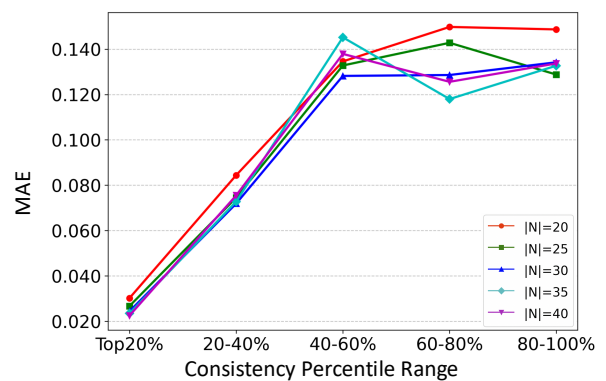
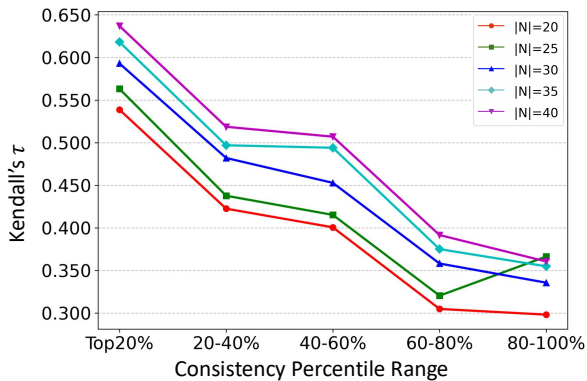


Figure 18: The impact of prediction consistency between the Native Source Model and Target Model (with quantity kept the same) on Winogrande benchmark.

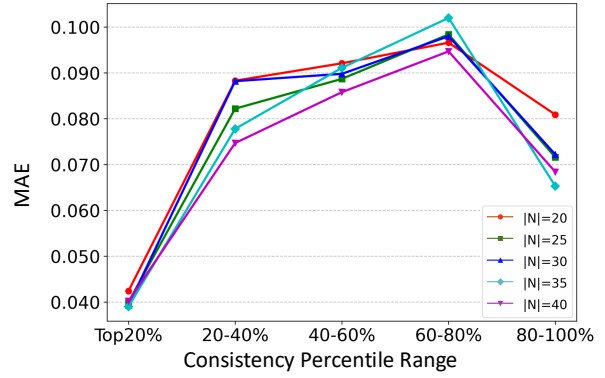
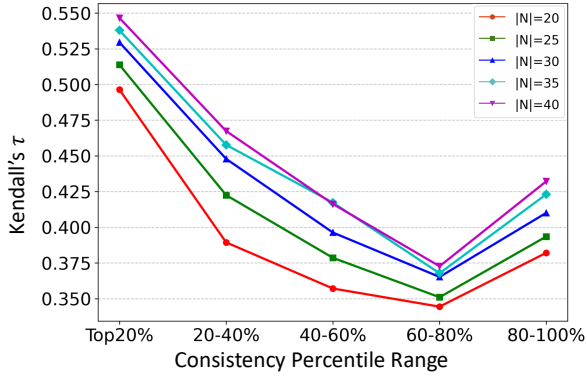


Figure 19: The impact of prediction consistency between the Native Source Model and Target Model (with quantity kept the same) on POPE benchmark.

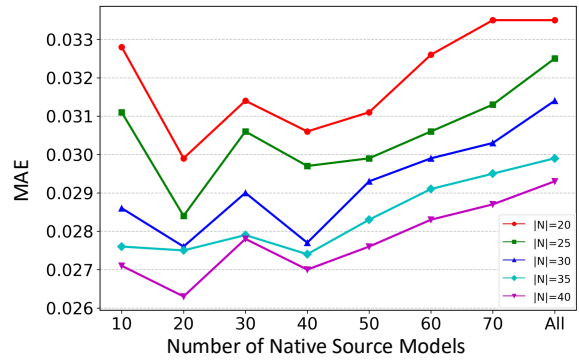
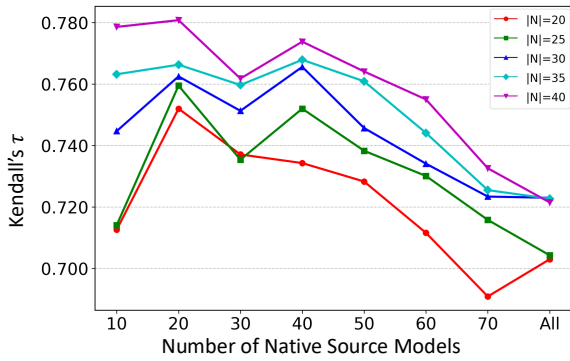


Figure 20: Performance of TAILOREDBENCH with varying numbers of Native Source Models on ARC Challenge benchmark.

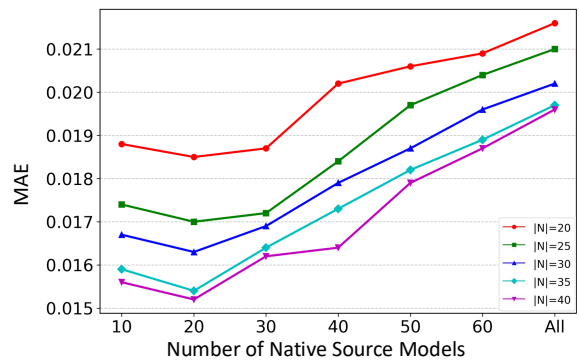
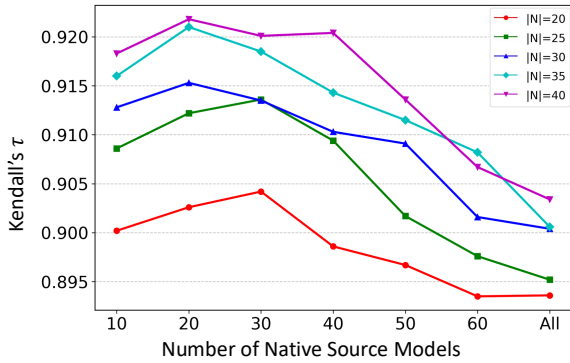


Figure 21: Performance of TAILOREDBENCH with varying numbers of Native Source Models on Hellaswag benchmark.

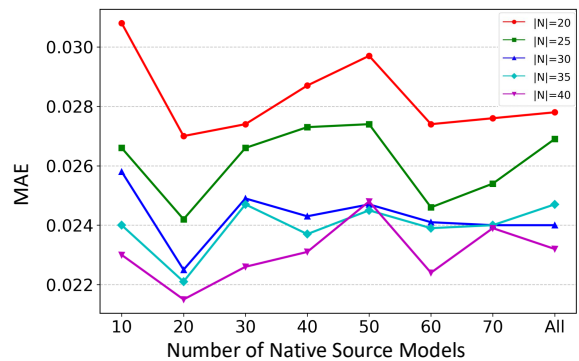
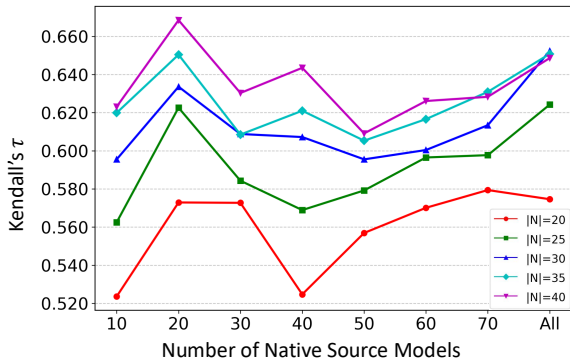


Figure 22: Performance of TAILOREDBENCH with varying numbers of Native Source Models on Winogrande benchmark.

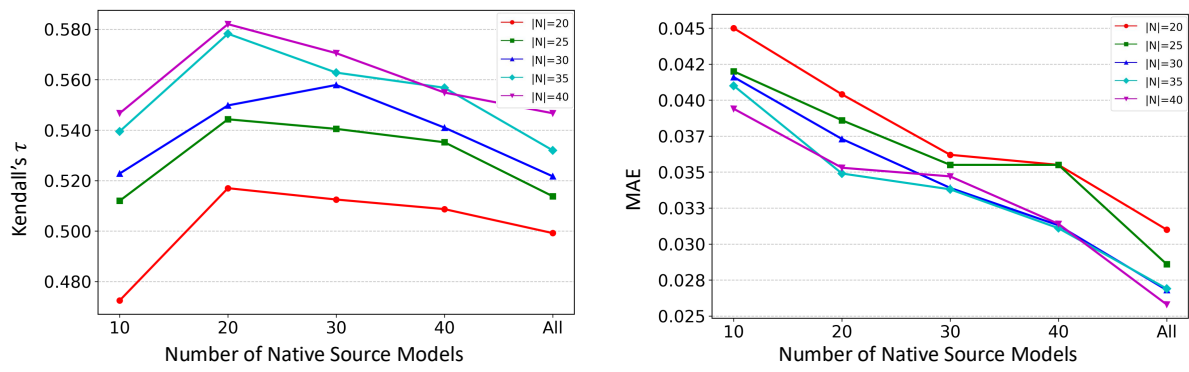


Figure 23: Performance of TAILOREDBENCH with varying numbers of Native Source Models on POPE benchmark.